

**EVALUATION OF L-BAND
BRIGHTNESS TEMPERATURE
PRODUCTS USING COMMUNITY
MICROWAVE EMISSION MODEL
AND SMAP BRIGHTNESS
TEMPERATURE OBSERVATIONS**


AMOS NYONGESA TABALIA

March, 2016

SUPERVISORS:

Dr. Y, Zeng

Dr. S, Lv



EVALUATION OF L-BAND BRIGHTNESS TEMPERATURE PRODUCTS USING COMMUNITY MICROWAVE EMISSION MODEL AND SMAP BRIGHTNESS TEMPERATURE OBSERVATIONS

AMOS NYONGESA TABALIA

Enschede, The Netherlands, [March, 2016]

Thesis submitted to the Faculty of Geo-Information Science and Earth Observation of the University of Twente in partial fulfilment of the requirements for the degree of Master of Science in Geo-information Science and Earth Observation.
Specialization: Water Resources and Environmental Management

SUPERVISORS:

Dr. Y, Zeng

Dr. S, Lv

THESIS ASSESSMENT BOARD:

Prof.Dr.Ing.Wouter Verhoeff (Chair)

Dr. Susan Steele-Dunne (External Examiner)

Dr. Yijian, Zeng (First Supervisor)

Dr. Shaoning, Lv (Second Supervisor)

Ir. Arno Vanlieshout (Course director)

DISCLAIMER

This document describes work undertaken as part of a programme of study at the Faculty of Geo-Information Science and Earth Observation of the University of Twente. All views and opinions expressed therein remain the sole responsibility of the author, and do not necessarily represent those of the Faculty.

ABSTRACT

This study describes the evaluation of the L-Band (1.4 GHz) brightness temperature from the microwave radiometer of the SMAP satellite mission by comparing it with ground-based modelled brightness temperature over the Maqu Soil Moisture and Soil Temperature (SMST) Monitoring network at Tibetan plateau. The ground-based modelled brightness temperature was calculated by CMEM (Community Microwave Emission Modelling Platform) model using in-situ SMST profile observations. The objectives of the study are: a) Model brightness temperature from soil moisture and soil temperature in-situ measurements in the Maqu catchment using the CMEM model; b) Use the L_v effective temperature scheme to understand the error characteristics of L-Band brightness temperature data from in-situ to network scale; c) Upscale point soil station data to field scale for matchup with SMAP satellite pixel scale; and d) Quantify the systematic and random errors of the SMAP brightness temperature product.

The CMEM physics is described in the ESA ECMWF contract document that documents implementation of the model as the SMOS forward operator. Using Soil moisture and soil temperature in-situ measurements from the Maqu SMST network and other ancillary datasets (leaf area index, skin temperature, air temperature at 2 metres and soil texture information) brightness temperature is modelled using different effective temperature parameterisation schemes.

Two methods of upscaling point soil moisture to field scale for matching with the SMAP satellite pixel scale are explored. The results of the study show that the simple average shows less residuals when compared to the weight functions as proposed by L_v . An analysis of the error contribution from each station when compared to the upscaled average shows that CST05 (4.6%) has less error contribution while NST08 (33.3%) has a higher error contribution to the total error budget.

L_v effective temperature scheme computes brightness temperature that has a better correlation with the SMAP satellite observation when compared to the other schemes. In the H polarization, L_v has a correlation of 0.25 compared to Choudhury (0.04), Wigneron (0.05) and Holmes (0.06). In the V polarization, L_v has a correlation of 0.26 compared to Choudhury (0.04), Wigneron (0.06) and Holmes (0.06). This research recommends further studies using the L_v scheme with different parameterisations for the other different modules of the CMEM. This will help to understand the sources of errors in CMEM modelling when compared to SMAP.

ACKNOWLEDGEMENTS

I would like to thank my supervisors Dr. Yijian Zeng and Shaoning Lv who have guided me through this difficult research for their flexibility in availing themselves to ensure that I succeed in this endeavour. Special recognition to Dr. Yijian for his encouragement especially when I had lost my confidence. Shaoning was very kind in helping circumnavigate the technical aspects of the thesis process. Thank you for these important gestures Dr. Yijian and Shaoning.

I acknowledge the role of the Dutch government through its Netherlands Fellowship Program for according me the opportunity to pursue my Master of Science education here. I also thank my employer, Nzoia Community Integrated Environmental Program for allowing me to pursue this master study and I believe that the knowledge gained will be important in ensuring that the organisation attains its goals.

I owe a lot of appreciation to the faculty of Geo-Information Science and Earth Observation and specifically the department of water and environmental management at the University of Twente for ensuring that the best education was available to me. Thank you to the staff for ensuring that we got the best training.

I would also like to specially thank my friends in ITC especially the water and environmental group for the friendship that they provided. The many friends I made during this process made the rigorous process manageable. The Kenyan community at ITC (Njuki, Kihara, Lilian, Githira, Kibet, Kasera and Grace) has a special place in my heart for all the help they provided in ensuring that we never missed home. Thank you to the group and thank you because you were the family away from home.

Lastly, I would like to acknowledge my parents and my siblings for the moral support they offered while I was away from home. I managed the long distance through the constant encouragement that they offered during this whole process. Thank you and God bless you abundantly.

TABLE OF CONTENTS

Abstract	iii
Acknowledgements	iv
List of figures	vii
List of tables	viii
Abbreviations	ix
1. Introduction.....	1
1.1. Theory and Background.....	1
1.1.1. Microwave Radiometry Physics.....	1
1.2. SMAP Mission	2
1.3. Problem Statement.....	3
1.4. Research Objectives.....	3
1.4.1. Specific Objectives.....	4
1.4.2. Research Questions	4
1.5. Research Relevance and Contribution.....	4
1.6. Study area.....	4
2. The CMEM Modelling.....	7
2.1. CMEM Physics	7
2.1.1. Soil module	8
2.1.2. Effective temperature.....	8
2.1.3. Soil roughness.....	9
2.1.4. Vegetation module.....	10
3. Modelling, upscaling and comparison of Brightness Temperature	11
3.1. Methodology	11
3.1.1. Input Data.....	12
3.1.2. Soil moisture and Soil temperature	12
3.1.3. Skin and Air temperature at 2 meter surface height.....	13
3.1.4. Vertical Discretization of the land Surface model in CMEM.....	14
3.1.5. Vegetation Effect.....	14
3.1.6. Soil and Sand	14
3.2. Upscaling of Point Brightness Temperature to Field Scale and Satellite Pixel Level.....	15
3.3. SMAP L1C Brightness Temperature	16
4. Results.....	17
4.1.1. Upscaling of point station data to pixel data.....	17
4.1.2. Comparison of different Effective Temperature schemes.....	18
4.1.3. Modelled TBH and TBV outputs based on the different effective temperature schemes	19
4.2. Matchup between CMEM and SMAP Brightness Temperature	20
5. Discussions	23
6. Conclusion and Recommendations	27
List of references	29
APPENDICES	32
Appendix A: Maqu network station characteristics	32
Appendix B: SMAP Satellite Overpass time.....	33
Appendix C: Weight functions based on Lv scheme (Lv et al., 2016).....	34
Appendix D: ECMWF-ECOCLIMAP Vegetation classification as adopted in CMEM	38
Appendix E: Residual error between individual stations TEFF and Weighted TEFF	39

Appendix F: Scatter plots for matchup between SMAP TB (H and V) and weighted model outputs..... 42
Appendix G: Scatter plots for matchup between SMAP TB (H and V) and a model outputs 43

LIST OF FIGURES

Figure 1: Contributions to TOA brightness temperature (SMOS ATBD, 2007)	2
Figure 2: Maqu SMST Network showing the stations location in a SMAP pixel	6
Figure 3: Flowchart of the methodology employed in the study.....	11
Figure 4: In-situ soil moisture measurements at different soil depths	13
Figure 5: Averaged in-situ Soil temperature measurements	13
Figure 6: ERA interim Reanalysis and Merra model data used for the period of study	14
Figure 7: Modelled point station Teff and Weighted Teff.....	17
Figure 8: Effective Temperature schemes simulations using simple average upscaling	18
Figure 9: Effective Temperature schemes simulations using weight functions upscaling.....	18
Figure 10: Comparison of simple upscaling versus Lv Weight functions upscaling	19
Figure 11: Effective Temperature schemes TBH outputs using weighted function upscaling.....	19
Figure 12: Effective Temperature schemes TBV outputs using Lv Weight functions upscaling.....	20
Figure 13: Lv scheme TBH using different upscaling approaches	20
Figure 14: SMAP versus simple average modelled TBH	21
Figure 15: SMAP versus weight function upscaling modelled TBH.....	21
Figure 16: SMAP versus simple average upscaling modelled TBV	21
Figure 17: SMAP versus weight function upscaling modelled TBV	22
Figure 18: Lv Scheme TBH and TBV with SMAP using different upscaling approaches	22
Figure 19: CST05 comparison with SMAP using the Lv scheme in the described study.....	24
Figure 20: CST05 comparison with SMAP using the Lv scheme in using C4 grassland.....	24
Figure 21: Latest RFI contaminated areas map from SMOS.....	26
Figure 22: Norm of residuals for individual stations	41
Figure 23: Scatter plots of SMAP TB against Weighted TEFF	42
Figure 24: Scatter plots of SMAP Tb versus Simple Average TEFF.....	43

LIST OF TABLES

Table 1: Modules of CMEM and the different Parameterisations	8
Table 2: Data sets from loggers and other sources for describing CMEM physics	12
Table 3: Adopted vertical discretization for the different soil layers	14
Table 4: Soil characteristics of four stations in the Maqu network	15
Table 5: Stations error contribution	17
Table 6: Statistical analysis of H-polarised modelled versus SMAP TBH	23
Table 7: Statistical analysis of V-polarised modelled versus SMAP TBV	23
Table 8: Maqu network station information (Su et al., 2011)	32
Table 9: SMAP Satellite overpass over the Maqu network during the Study period	33
Table 10: Vegetation classification for ECMWF-Ecoclimap	38

ABBREVIATIONS

ATBD	Algorithm Theoretical Basis Document
CMEM	Community Microwave Emission Modelling Platform
ECMWF	European Center for Medium-Range Weather Forecasting
ELBARA	ETH L-Band Radiometer for soil-moisture research.
EOS	Earth Observing System
ESA	European Space Agency
GEOS	Goddard Earth Observing System (model)
GMAO	Goddard Modeling and Assimilation Office
L0_TB	SMAP raw radiometer telemetry output data
L1C_TB	Converted radiometer data with geolocated brightness temperatures
L-Band	Microwave frequency at 1.4GHz
L-MEB	L-Band Emission of the Biosphere
L-SMEM	Land Surface Microwave Emission Model
LPRM	Land Parameter Retrieval Model
LSM	Land Surface Model
LTAN	Local Time Ascending Node
LTDN	Local Time Descending Node
NASA	National Aeronautics and Space Administration (United States space agency)
NCEP	National Centers for Environmental Prediction
NSIDC DAAC	National Snow and Ice Data Center Distributed Active Archive Center
NWP	Numerical Weather Prediction
RFI	Radio Frequency Interference
RMSE	Root Mean Square Error
SMAP	Soil Moisture Active Passive (NASA Space mission)
SMAPVEX	SMAP Validation EXperiment
SMDPC	Soil Moisture Data Processing Center
SMEX	Soil Moisture EXperiments (field campaigns)
SMOS	Soil Moisture Ocean Salinity (ESA Mission)
TB	Brightness Temperature
TOA	Top of the Atmosphere

1. INTRODUCTION

Surface soil moisture is a critical parameter in describing the water and energy exchanges between the atmosphere and the land surface interface. It determines the partitioning of the energy into sensible and latent heat fluctuation and as a soil state variable; it controls the partitioning of precipitation between runoff loss and infiltration storage. Intrinsically, surface soil moisture is an important element in the global circulation process and has been acknowledged as a parameter of vital potential for improving weather forecast and climate prediction (Fennessy & Shukla, 1999).

The use of hydrological models for extending the forecast of soil moisture over big areas is intricate and depends on the nature of the selected regions and available information on soil properties, such as permeability, hydraulic characteristics, meteorological and climatological data (Koster & Suarez, 1999). On the other hand, direct field measurements permit retrieval of precise approximations of soil moisture data in a concentrated spot and a lot of samples must be gathered to provide a representative sampling of the examined area (Newton, Heilman, & Van Bavel, 1983).

Thus, the prospect of employing remote sensing to monitor areas at global and regional scales rapidly and to measure integrated values of some geophysical parameters is important to soil moisture data users. An added advantage of remote sensing methods is the opportunity of examining the evolution in time of these parameters, which helps in improving hydrological model predictions using repeated satellite passages. The sensitivity of the electromagnetic radiation in the microwave band to the moisture of soil is a vital tool in global and local scale monitoring of soil moisture. Microwave sensors quantify the amount of microwave energy emitted (passive) or scattered (active) from land surface targets (Behari, 2005a). In soils, the detected energy intensity is linked to the quantity of moisture stored in the soil, although other site and location factors such as roughness and vegetation have an effect on emissions and scattering. Due to the sensitivity of microwaves to soil moisture, broad research efforts have been explored to develop ideal retrieval algorithms as well as to validate derived soil moisture products (EOportal Directory, 2014).

High-quality data and retrieval approaches that provide accurate soil moisture estimations are vital if soil moisture products from satellites are to be of meaningful value for global, regional, and national scales. Validation of the SMAP soil moisture products is an important mission obligation. Post-launch validation is concerned with product validation improvement, and further development (Piepmeier et al., 2014).

1.1. Theory and Background

1.1.1. Microwave Radiometry Physics

Passive microwave sensors detect and measure the natural thermal emission originating from the soil surface. The variation in the strength of this radiation is dependent on the dielectric characteristics and temperature of the object medium (Newton et al., 1983). For near surface soil layer dielectric properties are a function of the amount of moisture present (Simmer, 1999). Low microwave frequencies like the L-Band (1.4GHz) have the additional advantages of an almost complete transparent atmosphere which ensures the ability of all-weather detection (Parrens, Calvet, de Rosnay, & Decharme, 2014). Another advantage of L-Band frequencies is that transmission of signals from the underlying soil is probable through sparse and moderate vegetation layers (Wigneron et al., 2007). Lastly, L-Band microwaves are free from solar illumination, which permits day and night sensing (Johnson, 2012).

At microwave frequencies, the intensity of the observed emission (brightness temperature TB) is proportionate to the product of the temperature and emissivity of the surface based on the Rayleigh-Jeans

approximation theory. When the microwave sensor instrument orbits earth, the observed TB is a combined effect of a), energy emitted from soil and attenuated by superimposed vegetation, b) emission from the vegetation layer, c) the downwelling atmospheric emission and cosmic background emission reflected by the surface and attenuated by the vegetation, and the upwelling atmospheric emission (Kerr et al., 2001). The different interactions and contributions to the brightness temperature are in Figure 1.

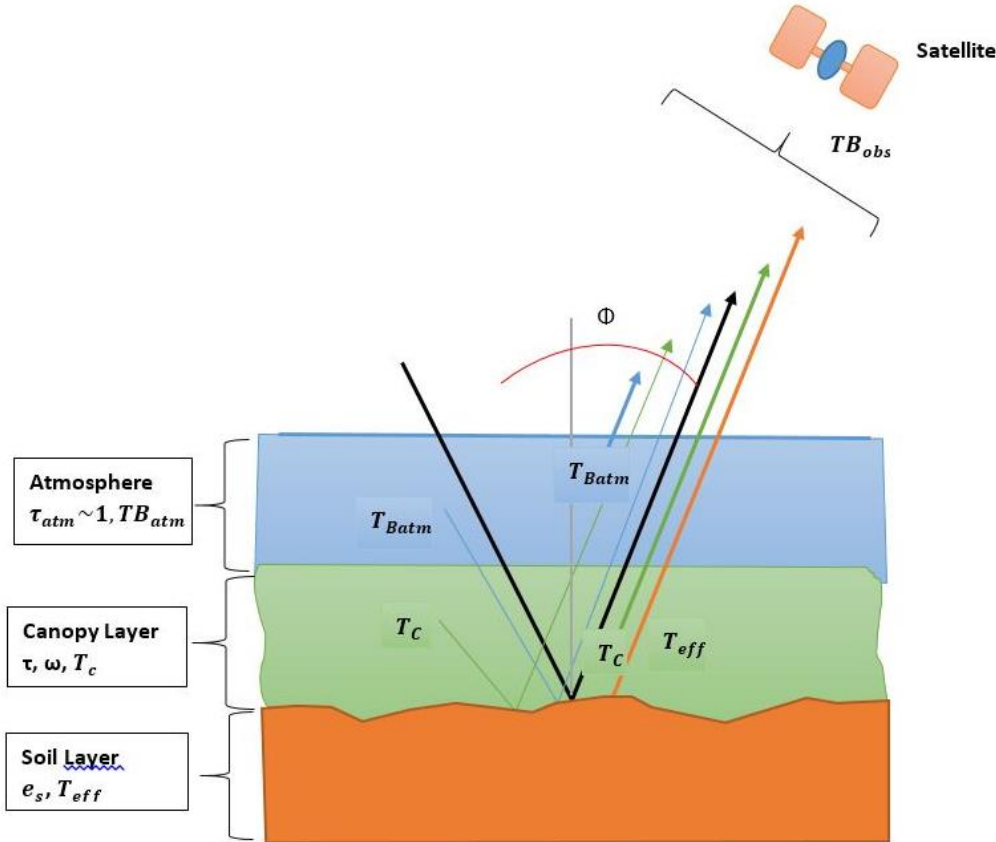


Figure 1: Contributions to TOA brightness temperature (SMOS ATBD, 2007)

1.2. SMAP Mission

The SMAP mission, launched in Jan. 31st 2015, has an overall objective of monitoring global soil moisture at high temporal and spatial resolution with an accuracy about $0.04 \text{ cm}^3/\text{cm}^3$. The novel approach of the SMAP radiometer instrument is its reflector antenna that guarantees that system calibration necessities are met (Neill, Chan, Njoku, Jackson, & Bindlish, 2012a). The reflector architecture is a mesh antenna with a diameter of 6 meters. Scientists have toyed with the idea of implementing large rotating antennas to increase the accuracy of L-Band remote sensing. The rotating reflector in a conical manner at nadir axis enables a 1000 km swath of observations at a 40-degree constant incidence angle. The rotating joint reflector optimises performance while reducing operation cost and risk (EOportal Directory, 2014; Miernecki et al., 2014; Neill, Chan, Njoku, Jackson, & Bindlish, 2012b; West, 2014).

The L-Band radiometer on-board SMAP provides global soil moisture products measured at 1.41GHz with the V, H, T3 and T4 polarisations in the top 5cm of the surface. Brightness temperature (L1C_TB) at a resolution of 36 km was provided with a latency of 50 hours (Neill, Chan, Njoku, Jackson, & Bindlish, 2012). The L-Band radiometer instrument requirements are polarizations in V, H, U a resolution of 36 km and

relative accuracy of 1.3 K. L1C_TB SMAP data requires calibration and validation data over locations where the grids coincide with time ordered locations.

Pre-launch calibration and validation field activities for the SMAP mission were carried out between 2008 and 2013. The SMAPVEX08 carried out on the US east coast was centred on resolving SMAP algorithm issues. The CanEx-SM10 in the Saskatchewan was done in conjunction with the Canadian L-Band radiometer where airborne radiometer measurements and in-situ sampling was done over four individual SMOS pixels (Magagi et al., 2013). Other field campaigns include the SMAPEX 1-3 designed to address SMAP soil moisture algorithm issues in three Australian fields (Panciera et al., 2014). SMAPVEX11 was carried out in Oklahoma to calibrate the SMAP atmospheric sensor (Jackson et al., 2012). SMAPVEX12 was another main pre-launch calibration and validation field campaign by NASA and the Canadian Space Agency. Validation site upscaling was one of the most important targets of the SMAPVEX12 campaign (McNairn et al., 2015).

1.3. Problem Statement

Soil moisture is an important parameter for Numerical Weather Prediction where it provides initial conditions for the land surface boundary conditions. Ground networks, which require high investment and maintenance cost, provide ideal in-situ soil moisture measurements. High cost of maintenance makes it impossible to provide global coverage of soil moisture networks (Behari, 2005b). Scarcity of ground soil moisture has resulted in the use of radar and radiometer sensors aboard satellites. Satellites such as SMOS and SMAP offer a high global coverage of soil moisture products. Soil moisture products from satellites provide data at a global scale and a consistent revisit time. Nevertheless, the coarse spatial resolution brightness temperature from satellites may result in errors not desired by users. Spatial-temporal variability due to atmospheric conditions, land cover, heterogeneity of properties of the soil, vegetation and surface topography affects the accuracy of the retrieved brightness temperature (Su et al., 2011).

Users and scientists have developed and applied different algorithms at local scales using modelling the land surface and atmospheric variables, parameters, and combining them with satellite measurements to improve accuracy and resolution of satellite products. This has been done to give a suitable temporal scale of soil moisture. However, operational application of algorithms at regional scales using satellite sensor measurements suffer from shortage of information regarding numerous parameters involved in radiometry physics and the high spatial heterogeneity within the footprint of land surface variables.

In-situ measurements from ground radiometer instruments such as the ELBARA are ideal observations that provide accurate brightness temperatures at point scale ideal for validating satellite brightness temperature (Jackson et al., 2012). It is important to upscale in-situ instrument measurements to the satellite pixel scale for the measurement to be useful in validation of satellite products. The process of upscaling a point measurement scale in the array of metres to the size of a satellite pixel scale in the range of tens of kilometres introduces uncertainties (De Lannoy et al., 2007).

For SMAP Brightness temperature to be useful at regional and local scales there is need to test and define uncertainties that are observed in the algorithms using the forward operator (i.e. CMEM) and in-situ observations. Calibrating and validating brightness temperature products using in-situ measurements is critical in provision of reliable soil moisture products (Su et al., 2011).

1.4. Research Objectives

The main objective of this study is to evaluate brightness temperature products in the Maqu network through modelling of in-situ brightness temperature and using it to validate SMAP Level 1C brightness Temperature products (L1C_Tb).

1.4.1. Specific Objectives

- Model brightness temperature from soil moisture and soil temperature in-situ measurements in Maqu network using the CMEM model.
- Apply the new soil effective temperature scheme (Lv, Wen, Zeng, Tian, & Su, 2014) in the CMEM over the Tibetan plateau.
- Upscale point soil moisture to SMAP satellite pixel scale
- Identify uncertainties of SMAP TB products over the Maqu network.

1.4.2. Research Questions

- How do land surface heterogeneity affect the CMEM in simulating brightness temperature?
- What is the error character between modelled brightness temperature from different effective temperature schemes and the observed SMAP brightness temperature?
- What is the best approach to upscale point brightness temperature to SMAP pixel?
- What are the sources of uncertainties between modelled brightness temperature and the observed SMAP brightness temperature?

1.5. Research Relevance and Contribution

The research is important for SMAP science users to understand and reduce the sources of uncertainties of brightness temperature (TB) retrieval over the high latitude regions (e.g. over the Maqu catchment in Tibet region and other regions with similar hydro-climatic conditions). Successful implementation of the model provides insight into how SMAP TB can be used to derive soil moisture through inverse modelling. The SMAP scientific team has also indicated the need to use a more comprehensive effective temperature scheme in their retrieval algorithm. Through evaluation of the different effective temperature schemes in this study, an insight into the most appropriate effective temperature is offered. The study implements the two-layered effective temperature scheme (LV, 2014) in the CMEM model in calibrating and validating the SMAP observation using modelled brightness temperature, at the meantime, examining the sensitivity of the modelled Tb to different effective temperature schemes.

1.6. Study area

The Maqu soil moisture and soil temperature network is located at the north-eastern edge of the Tibetan Plateau (33.300–34.150 N, 101.380–102.450 E) and at the first major meander between the Yellow and Black river. It covers the large valley of the river and the surrounding hills, with a uniform short grassland cover. The elevations of the stations range between 3430 m and 3752 m above mean sea level including typical landscapes with hills, valleys, river, wetlands, grassland and bare soil zones. Organic soil wetlands characterize a large part of the valley, while silt loam soils are observed on the hills. According to the Koeppen Classification System, the climate at this site is defined by rainy summers and dry winters due to the monsoon winds network. The network, consisting of 20 stations in an area of approximately 40 km by 80 km, monitors continuously the soil moisture and soil temperature at different depths (from 5 to 80 cm below surface) at 15 min intervals (Su et al., 2011). Figure 2 shows the location of Maqu soil moisture network in the Tibetan plateau observatory with the exact location of the eight stations used in this study in the SMAP pixel.

Su et al. (2011) demonstrate the unique nature of the Tibetan Plateau networks in quantifying errors in coarse soil moisture products. These characteristics are ideal for vegetation cover correction, surface terrain correction and soil heterogeneity correction, which are important parameters for the CMEM model. The study (Su et al., 2011) concludes that the coarse global resolution of soil moisture products are useful but they exhibit unprecedented uncertainties in cold and semi-arid regions like the Tibetan Plateau observatory.

The Maqu soil network stations locations are chosen to monitor the area comprehensively at diverse altitudes and for different soil characteristics. Appendix A is a summary of the stations based on their elevations, land cover characteristics, depth of probes, the locations topography and geographical coordinates (Su et al., 2011). The soil probe used for recording data is the capacitance EC-TM ECH2O which consists of three 5.2 cm flat pins measuring the dielectric permittivity of the soil next to the pins hence providing volumetric soil moisture. Soil temperature is estimated using a thermistor on the probe. Organic matter content, bulk density and particle size distribution were estimated during the installation process by taking soil sample estimates (Su et al., 2011).

Su et al., (2011) noted that because the dielectric properties of soils depend on soil texture and salinity, calibration for soils in Maqu was carried out using soil rings, with which the uncertainty of approximately 3% given by the generic calibration equation (default by the datalogger) valid for all fine textured mineral soils can be reduced to 1–2 %. The calibration methodology abridged RMSD between the volumetric soil moisture measured by the rings and that by the probes from 0.06 to 0.02 m³ m⁻³, which can be considered as the absolute accuracy of each station in the network (Dente et al., 2012)

EVALUATION OF L-BAND BRIGHTNESS TEMPERATURE PRODUCTS USING CMEM MODELLED IN-SITU OBSERVATIONS AND SMAP BRIGHTNESS TEMPERATURE

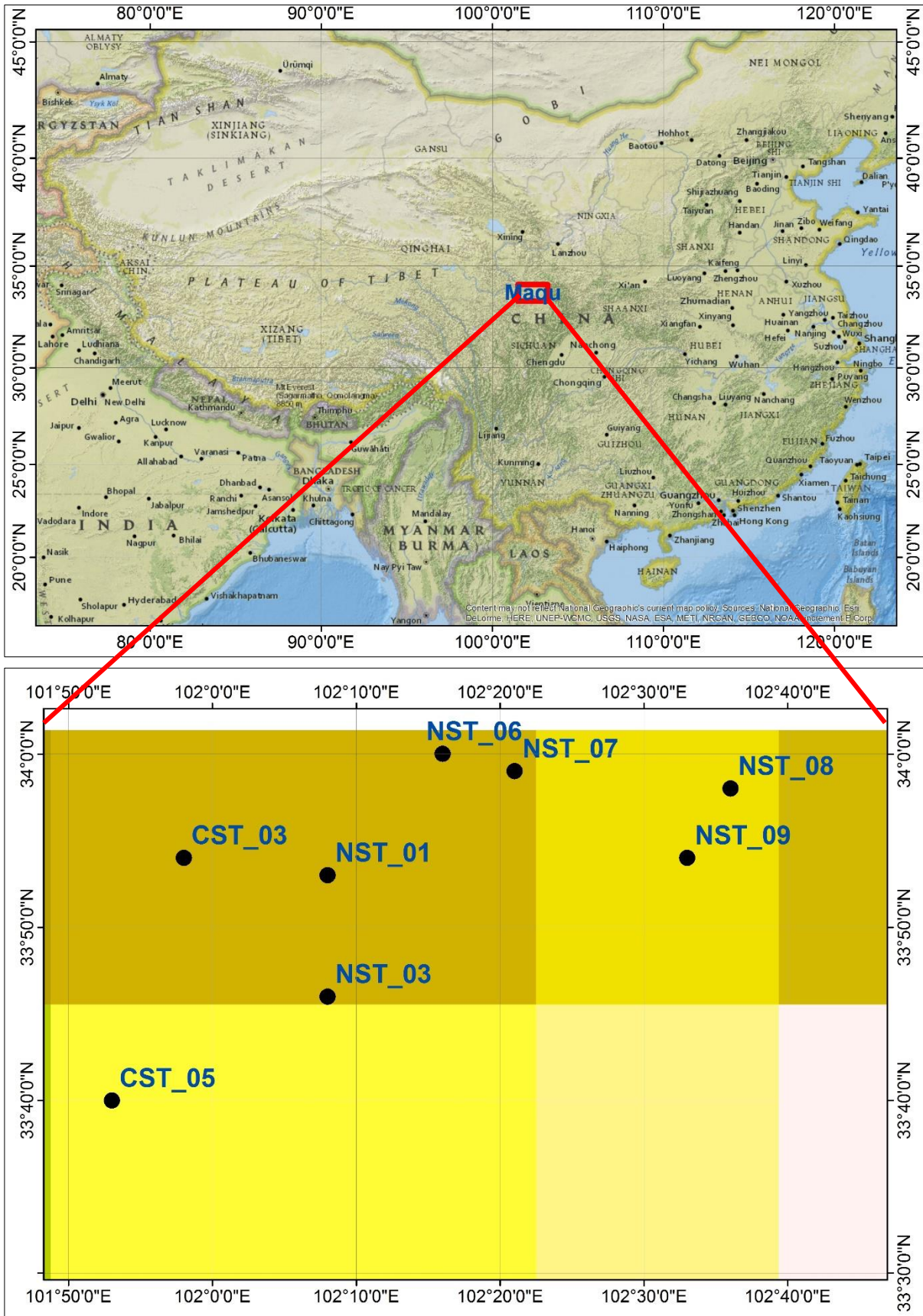


Figure 2: Maqu SMST Network showing the stations location in a SMAP pixel

2. THE CMEM MODELLING

Several studies have been carried out to obtain soil moisture estimates from satellite microwave radiometer (Wigneron et al., 2007; De Lannoy, Reichle, & Pauwels, 2013 and Zeng et al., 2015). The current CMEM (Community Microwave Emission Modelling Platform) model (De Rosnay et al., 2009) is ideal for the retrieval of brightness temperature at low frequencies of between 1.4 GHz-20GHz, which is subsequently used to retrieve soil moisture products. The CMEM was also designed to be used as a forward operator for computing Top of the Atmosphere (TOA) brightness temperature in the ECMWF NWP model interface (De Rosnay, Drusch, & Sabater, 2009). The forward operator was mainly applied in deriving brightness temperature for the SMOS mission (De Lannoy et al., 2013 and Parrens, Calvet, de Rosnay, & Decharme, 2014). The model is a hybrid version of the L-MEB and LSMEM and it consists of four components that compute surface brightness temperature for soil, vegetation brightness temperature, snow modifications and atmosphere brightness temperature (De Rosnay et al., 2009). The CMEM modular model combines different parameterisations that compute surface and atmospheric emissions. These are the soil dielectric mixing model, effective temperature model, soil roughness model, smooth surface emissivity model, vegetation opacity model and the atmospheric radiative transfer model (De Rosnay et al., 2009).

2.1. CMEM Physics

The methodology employed for CMEM modelling is described by (De Rosnay, Drusch, & Sabater, 2009) in the ESA contract report (De Rosnay et al., 2009). The CMEM modular includes the physics and parameterizations that are used in the LSMEM (Drusch et al. 2001) and the L-MEB (Wigneron et al. 2007). The basis of the theory in CMEM is a simplified solution of the vector radiative transfer equation (Kerr & Njoku 1990 and Drusch & Crewell 2005). Brightness temperature in areas with no snow at TOA $T_{Btoa,p}$, where p stands for the polarisation, is expressed as shown in the equation 2-1 and 2-2 below

$$T_{Btoa,p} = T_{Bau,p} + \exp(-\tau_{atm,p})T_{Btov,p} \quad 2-1$$

$$T_{Btov,p} = T_{Bsoil,p} \exp(-\tau_{veg,p}) + T_{Bveg,p} [1 + r_{r,p} \exp(-\tau_{veg,p})] + T_{Bad,p} r_{r,p} \exp(-2 \cdot \tau_{veg,p}) \quad 2-2$$

Where

$T_{Bau,p}$ = Upwelling atmospheric emission.

$\tau_{atm,p}$ = Atmospheric optical depth.

$T_{Btov,p}$ = Top of vegetation brightness temperature with vegetation as a single-scattering layer above a rough surface.

$T_{Bsoil,p}$ = Soil layer contribution.

$T_{Bveg,p}$ = Vegetation layer contribution.

$T_{Bad,p}$ = Downward atmospheric contributions.

$r_{r,p}$ = Soil reflectivity of the rough surface ($1 - \epsilon_{r,p}$).

$\tau_{veg,p}$ = Vegetation optical depth along the viewing path.

The CMEM model consists of four modules that calculate contributions from soil, vegetation, snow and the atmosphere. This study assumes that there was no snow cover between during the period of study from 2015-04-01 to 2015-07-01. Hence only three modules are considered in the modelling process. The code is segmented to compute each microwave modelling component by offering a choice of several parameterizations. Table 1 is a summary of the segmented structure of the model with a list of the options that can be executed (De Rosnay et al., 2009).

Table 1: Modules of CMEM and the different Parameterisations

Module	Variable	Parameterisation
Soil	ϵ	Wang & Schmugge (1980) Dobson et al. (1985) Mironov et al. (2004)
	T_{eff}	Choudhury et al. (1982) Holmes et al. (2006) Wigneron et al. (2001) and Lv Scheme
	$e_{s,p}$	Fresnel law and Wilheit (1978)
	$e_{r,p}$	Choudhury et al. (1979) Wigneron et al. (2001) SMOS ATBD (2007) Wegmuller & Matzler(1999) Wigneron et al. (2007)
Vegetation	$\tau_{veg,p}$	Wegmuller et al. (1995), Wsimple(Wigneron et al. (2007)) , Kirdyashev et al. (1979) Jackson & O'Neill(1990).
Atmosphere	$\tau_{atm,p}$	Pellarin et al. (2002) Liebe (2004) Ulaby et al. (1986)

2.1.1. Soil module

The soil element of CMEM includes four components to compute the soil dielectric constant ϵ , the effective temperature $T_{Bsoil,p}$, smooth soil emissivity $e_{s,p}$ and rough soil emissivity $e_{r,p}$. Based on the Rayleigh-Jeans approximation for the microwave domain the soil brightness temperature is expressed as a product of soil emissivity $e_{r,p}$ and effective temperature (De Rosnay et al., 2009).

$$T_{Bsoil,p} = T_{eff} \cdot e_{r,p} \quad 2-3$$

2.1.2. Effective temperature

The main surface variable that should be accounted during retrieval and modelling of soil moisture in L-Band frequencies is the effective temperature (T_{eff}). Effective temperature schemes play a major role in determining the brightness temperature in forward modelling. At L-Band frequencies, soil temperature varies with sensing depth and is different from the temperature of the vegetation. T_{eff} Schemes work on the assumption that both soil moisture and soil temperature should be homogeneous in the first layer and in the deeper layer(LV et al, 2014).

The Wilheit model (1978) estimates effective temperature using a weighting function on all soil layers. The disadvantage with the Wilheit model is that it is computationally costly (Wilheit, 1978). To reduce this cost, effective temperature can be parameterized based on surface layer temperature at 5cm and deep layered soil temperatures at 50cm, 80cm or even 2m (De Rosnay et al., 2009; Holmes, 2006; Njoku & Entekhabi, 1996).

$$T_{eff} = T_{deep} + C(T_{surf} - T_{deep}) \quad 2-4$$

The C parameter is correlated to temperature sensing depth and different authors have used different approaches to calibrate the C parameter. The Choudhury scheme is not soil dependent and hence it considers the soil moisture as a single layer based on the soil temperature (De Rosnay et al., 2008). The homogenous approach of Choudhury scheme in estimating effective temperature tends to lead to a high

estimation of effective temperature, which results in underestimation of brightness temperature. Hence, Choudhury assumes a Constant C parameter for frequencies 0.6-10 GHz (Choudhury et al., 1982). The Wigneron effective temperature scheme is an adaptation of the Choudhury model to account for soil moisture influence on the effective temperature. Thus, Wigneron calibrates a moisture dependent C parameter for frequencies of 1.4 GHz (Wigneron et al., 2001). The Holmes scheme is based on the use of the Wang dielectric constant to model soil moisture dependence on sensing depth. The Wang dielectric model employs the concept of non-linear variation between sensing depth and soil moisture (De Rosnay et al., 2008). This implies that the Holmes scheme assumes a dielectric constant dependent C parameter for frequencies of 1.4 GHz (Holmes et al., 2006).

Lv's scheme is capable of providing T_{eff} with a physical base. The two layered scheme discrete procedure has a clear physical implication, which allows for all measurements made in the soil column to be unified in order to attain a more accurate T_{eff} , without disturbing the original part concerning the top soil layer, and only adapting the weights for the residual errors linked to deeper soil layers. An accurate T_{eff} could be computed from observations of each layer (Lv et al., 2014).

The Lv's scheme computes effective temperature as shown by equation 2-5.

$$T_{eff} = T_1(1 - e^{-B_1}) + T_2 e^{-B_1} \quad 2-5$$

Where $B_1 = \alpha_1 x_1$

In this context, x is the vertical distance (depth) where physical temperature is measured and $\alpha_1 x_1$ is an attenuation coefficient determined by dielectric constant ϵ and wavelength λ . The detailed form of $\alpha(x)$ is described by (Wilheit, 1978). The C parameter from Choudhury et al., 1982, can be described as shown below in the Lv Scheme (Lv et al., 2014).

$$c = 1 - e^{-B_1} = 1 - \exp\left(-\Delta x \cdot \frac{4\pi}{\lambda} \cdot \frac{\epsilon''}{2\sqrt{\epsilon'}}\right) \quad 2-6$$

2.1.3. Soil roughness

The semi-empirical approach proposed by Wang and Choudhry, (1981) to represent soil roughness effects on the microwave emission computes rough emissivity as a function of smooth emissivity and three other parameters Q , h , N :

$$r_{r,p} = [Qr_{s,p} + (1 - Q)r_{s,q}] \exp(-h \cos^N \varphi) \quad 2-7$$

In this context, p and q represents the polarization states, Q is the polarization mixing factor, N designates the angular dependency, h is roughness parameter, and φ is defined as the incidence angle. Wigneron et al. 2007 and Njoku, Jackson, Lakshmi, Chan, & Nghiem, 2003 consider the mixing factor Q as being very low at low frequencies and is generally set to 0 (De Rosnay et al., 2009).

For the roughness parameter h , a number of parameterizations exist. They are based on

- (i) Wavenumber, empirical coefficients, and the rms surface height σ (Choudhury, Schmugge, Chang, & Newton, 1979 and Wegmüller & Matzler, 1999)
- (ii) Empirical coefficients, correlation length, wavenumber, the rms surface height, and (Wigneron, Laguerre, & Kerr, 2001)

- (iii) Soil moisture and soil texture or
- (iv) Soil moisture and vegetation type (Wigneron et al. 2007).

2.1.4. Vegetation module

In CMEM, vegetation is calculated by the $\tau - \omega$ approaches where the vegetation layer has a clear influence to the TOA signal and reduces the emission from the underlying soil (Schmugge, O'Neill, & Wang, 1986).

$$T_{Bveg,p} = T_c(1 - \omega_p)[1 - \exp(-\tau_{veg,p})] \quad 2-8$$

T_c is the canopy temperature

ω_p is the single scattering albedo at polarization p .

With equation 2-8, Jackson & Schmugge, (1991) propose a simple parameterization to compute the vegetation optical thickness as shown in equation 2-9.

$$T_{Bveg,p} = b \frac{VWC}{\cos\varphi} \quad 2-9$$

From equation 2-9, b and VWC is the vegetation layer parameter and the vegetation water content, respectively. The single scattering albedo is presumed static at $\omega = 0.05$ for low vegetation types (grass and crops) and for high vegetation types (forests) (De Rosnay et al., 2009).

The Wigneron et al. (2007) vegetation optical thickness model also describes the vegetation effect with equation 2-9. In their formulation, the single scattering albedo depends on vegetation type and polarization. The polarized optical thickness is expressed as shown in equation 2-10 and 2-11.

$$T_{Bveg,p} = \tau_{nadir}(\cos^2 + tt_p \sin^2 \varphi) \frac{1}{\cos \varphi} \quad 2-10$$

$$\tau_{nadir} = b' LAI + b'' \quad 2-11$$

$$\tau_{nadir} = b''' \quad 2-12$$

Equation 2-10 is for high vegetation. Here, tt_p parameters characterise the angular consequence on vegetation optical thickness for each vector of polarisation and vegetation categories (at nadir, tt_p has no effect on the simulations). The vegetation layer parameters b' , b'' , and b''' and the single scattering albedo are acquired based on lookup tables in several databases (Wigneron et al. 2007).

The Kirdyashev et al. (1979) parameterization computes optical thickness of the vegetation as a part of the wavenumber k (between 1 and 7.5GHz), the dielectric constant of saline water, ϵ_{sw}'' (imaginary part), VWC, incidence angle ψ , water density ρ_{waters} , and a vegetation structure parameter a_{geo} :

$$T_{veg,p} = a_{geo} k \frac{VWC}{\rho_{water}} \epsilon_{sw}'' \frac{1}{\cos\varphi} \quad 2-13$$

The assumption made in equation 2-13 is that the single scattering albedo is constant at $\omega = 0.05$. $T_{Bveg,p}$ is computed for each model grid box, while accounting for the sub grid-scale variability of the land surface. CMEM grid box can account up to seven-grid box at a single moment: bare soil, low vegetation, high vegetation and open water as shown in Table 10 in Appendix D. In order to compute the vegetation tiles, the dominant vegetation class is acquired from an ancillary land-use classification dataset (De Rosnay et al., 2009).

3. MODELLING, UPSCALING AND COMPARISON OF BRIGHTNESS TEMPERATURE

3.1. Methodology

Soil moisture and soil temperature in-situ measurements for the period 2015-4-01 to 2015-07-12 are modelled for eight stations in the network. The data used is from station CST03, CST05, NST01, NST03, NST06, NST07, NST08, and NST09. The process employed by this study in attaining the set objectives is shown in Figure 3.

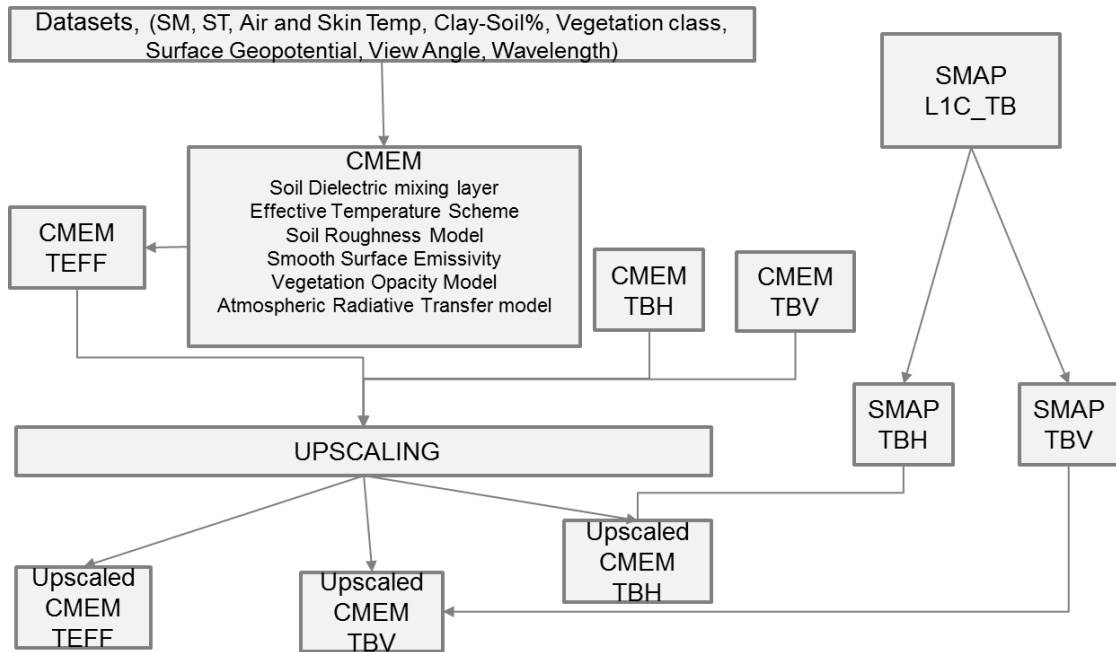


Figure 3: Flowchart of the methodology employed in the study

The input datasets as described in 3.1.1 below are prepared for CMEM model runs. The CMEM platform is coded in Fortran 90 and with three different options for file inputs. This include different forcing inputs and output file templates. The forcing files can be used as either Grib, ASCII or Netcdf files. Grib files provide the advantage of gridded data from various NWP, which provide gridded data. The ASCII option has the advantage of handling inputs from field measurements and less computing energy due to single pixel estimation. The ASCII option was chosen for this study because of the need to calculate outputs at pixel level and at the same time to input field retrieved soil texture, soil moisture and soil temperature measurements.

In order to successfully decode and run the model, the Linux environment has to be created that provides ease of manipulation of different subroutines using the command terminal. Several packages that support the model configuration were installed to enable the required Linux environment for the decoding and manipulation of the model and the different subroutine. The Fortran 90/95 compiler was installed and in Ubuntu, gfortran from the software centre was used. Ubuntu has a c compiler, gcc and a C++ compiler g++, which are easily installed. The CMEM is then run by compiling the model with all the input files using the 'Make' to update the makefile and then using './CMEM' to run the whole module.

This research employs the default CMEM parameterisation from ECMWF the default dielectric parameterisation is the Wang & Schmugge (1980). Fresnel law theory is used to calculate the smooth surface emissivity while the Wsimple model parameterises soil roughness option Wigneron (2007) method is applied for vegetation opacity option and the Pellarin parameterisation is used for the atmospheric option. Because the objective of this study is to study the different effective temperature parameterisations, Choudhry, Wigneron, Lv and Holmes schemes are used with data from the eight soil stations in the Maqu network.

The three outputs from the CMEM model, Effective Temperature (TEFF), Brightness temperature in horizontal polarisation (CMEM TBH) and Brightness temperature in the vertical polarisation (CMEM TBV) are then upscaled by use of the two methods described in 3.2 below. The upscaled products from the CMEM are then compared to the SMAP Brightness temperature in horizontal polarisation (SMAP TBH) and Brightness temperature in the vertical polarisation (SMAP TBV).

3.1.1. Input Data

To simulate CMEM brightness temperatures, a time series of soil moisture and soil temperature at different depths is required. The datasets used for this study from the Maqu network are for the period between 1st April 2015 and 1st July 2015 at 6.00am every day. This is to coincide with the SMAP satellite overpass times. Table 2 shows datasets and their sources.

Table 2: Data sets from loggers and other sources for describing CMEM physics

CMEM Modelling DATA Requirements	
Soil Moisture layer 5, 10, 20, 40, 80	From Maqu SMST network
Soil Temperature layer 5, 10, 20, 40, 80	From Maqu SMST network
Air temperature at 2m	From ERA-Interim Reanalysis data
Surface Skin temperature	From ERA-Interim Reanalysis data

3.1.2. Soil moisture and Soil temperature

All the 19 stations in the Maqu network have been fitted with ECT soil moisture probes at different depths. The physical mounting depths of soil moisture/soil temperature probes for each stations are shown in Table 9. This study uses only data from eight stations because available data for the 2015 period was from eleven stations. Three of the 11 stations had missing datasets which after screening, it was clear they would have a big error on the combined model output. The postulation from the screening of the data was that either the three stations had broken sensors or the functionality of the sensors was compromised.

An example of the SM/ST measurements in the CST03 is shown in Figure 4 and Figure 5. CST03 has soil moisture and soil temperature probes fitted at 5cm, 10cm, 20cm, 40cm, and 80cm depths. In figure 5, the soil moisture at depth 5 cm generally shows more variability compared to the other layers. The measurements at depth 40cm are less variable while measurements at depth 10 and 20 and 80 have less change over time during the study period.

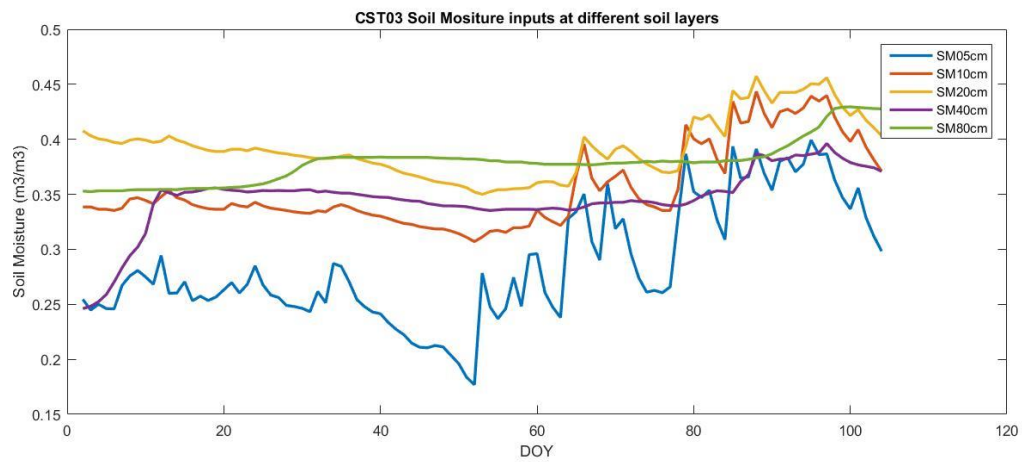


Figure 4: In-situ soil moisture measurements at different soil depths

Figure 5 shows the soil temperature measurements at different depths in CST03. The measurements of soil temperature at depth 5cm, 10cm, and 20cm show more variability with time compared to measurements at depth 40cm and 80cm. Based on the in-situ measurements it can be proposed that soil temperature measurements capture variability at different depths more accurately compared to soil moisture measurements.

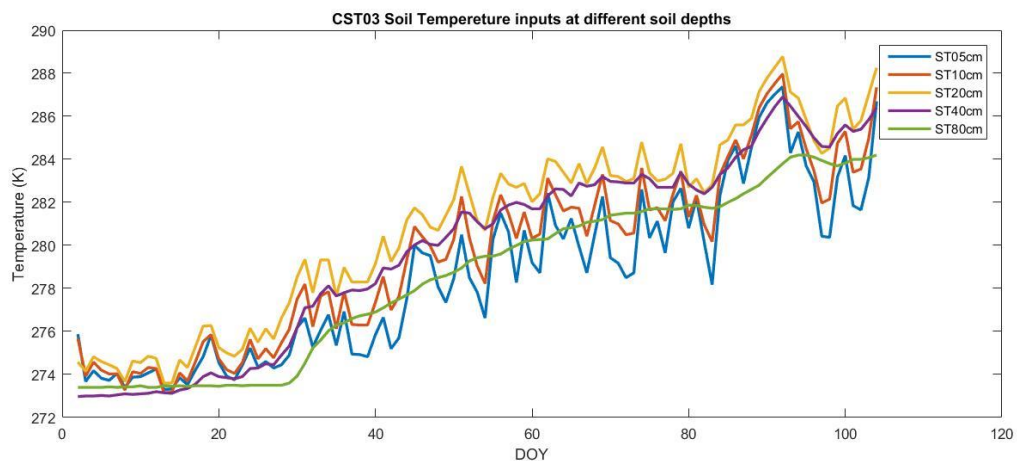


Figure 5: Averaged in-situ Soil temperature measurements

3.1.3. Skin and Air temperature at 2 meter surface height

Air temperature at 2meters and Surface skin temperature of the network are used in the model structure as proxy datasets for the model to be able to compute soil temperatures. Lack of in-situ measurement data is overcome by use of online database sources. ERA-Interim reanalysis data is used as model forcing for Surface skin temperature and Air temperature at 2 meters. Figure 6 shows the time series plots of the air temperature at 2meters and Skin temperature of the Maqu network during the study period 2015-04-01 to 2015-07-01. ERA-Interim reanalysis data is an hourly product and for this study, measurements at 6.00am are taken to coincide with the in-situ soil moisture and soil temperature measurements at 6.00am for the modelling process. The SMAP L1C_TB products used are for 6.00am and by ensuring that the model forcing is correct, the matchup between the two will reduce errors.

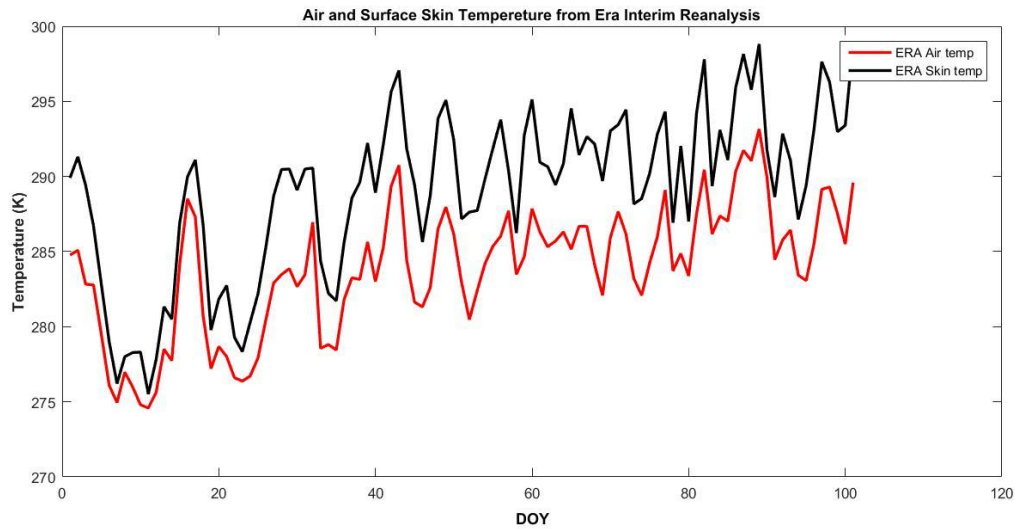


Figure 6: ERA interim Reanalysis and Merra model data used for the period of study

3.1.4. Vertical Discretization of the land Surface model in CMEM

The LSM vertical resolution for soil moisture and soil temperature measurements is an important factor in ensuring that the model runs as per the requirements. The specific depths for the ECT probes are 5cm, 10cm, 20cm, 40cm and 80 cm. These depths define the number of layers that the model will take. Some stations have data for all the five layers while others have four, three, two, and one layer datasets. For each specific layer, an LSM vertical resolution is defined based on the number of layers. Table 3 below shows the adopted LSM vertical resolution which has to be defined in the model structure.

Table 3: Adopted vertical discretization for the different soil layers

Layer Depth	LSM Vertical resolution
0-5cm	0.025
5-10cm	0.075
10-20cm	0.15
20-40cm	0.30
40-80cm	0.60

3.1.5. Vegetation Effect

The model uses different parameterization in modelling the vegetation effect on the emissions from the soil and water layer. This determines the type of data that is required to compute the vegetation effect. In the setup used, the ECOCLIMAP-ECMWF vegetation classification as shown in Table 10 is used. A value for the low vegetation and high vegetation is used to model the vegetation effect. Based on this, the Maqu network is classified as having low vegetation C3 grasslands.

3.1.6. Soil and Sand

An important dataset for the model to work is the soil conditions, which is defined by the soil texture data. In this case based on field experiments carried out by Zheng, (2015), an average of the sand and clay percentages is used. Sand and Clay percentages for each station are provided as inputs with the specific geopotential height at surface. Table 4 below shows the sand and clay percentages of sample stations based on Zheng, (2015).

Table 4: Soil characteristics of four stations in the Maqu network

Site	Depth	Sand	Clay	Texture
CST01	5-15	34.78	9.38	Silt Loam
	20-40a	39.49	9.01	Silt Loam
	20-40b	65.56	5.45	Sandy Loam
	55-70	57.92	6.65	Sandy Loam
NST01	5-15	36.07	7.42	Silt Loam
	20-40	52.33	6.65	Sandy Loam
	55-70	61.24	5.92	Sandy Loam
NST04	5-15	36.57	7.10	Organic Soil
	20-40	27.29	8.94	Organic Soil
	55-70	18.24	9.42	Silt Loam
NST11	5-15	18.56	9.01	Organic Soil
	20-40	30.17	11.01	Silt Loam
	55-70a	29.16	11.22	Silt Loam
	55-70b	48.05	6.01	Sandy Loam

3.2. Upscaling of Point Brightness Temperature to Field Scale and Satellite Pixel Level

The model outputs for the period 2015-04-01 to 2015-07-01 are used to compute the network TBH and TBV to provide a single pixel value to represents the Maqu network. Two methods are proposed in this study. The first method involves an average of all the eight station where a summation of all the station is divided by the number of stations. This is shown by the equation 3-1 below.

$$TB_A = \frac{1}{n} \times \sum_{i=1}^n TB_i \quad 3-1$$

Where, TB_A is the average brightness temperature, TB_i is the brightness temperature of an individual station and n is the number of stations.

The second method is the Lv weight functions, which considers the weights of each station (Lv, Zeng, WEN, ZHENG, & SU, 2016) to provide a field scale TBH and TBV respectively. The weight functions for each station are shown in Table 2 (Appendix C). The method infers that to estimate T_{eff} with utmost accuracy, the physical mounting depth of the SMST probes should be designed to have minimal residual effect as possible (e.g. the emission from the rest of soil layer can be neglected). Implementation of the weight functions is shown in the equation 3-2.

$$TB_A = \frac{1}{\sum_{i=1}^n W_i} \times \sum_{i=1}^n (W_i \times TB_i) \quad 3-2$$

Where TB_A is the new spatial average Brightness temperature, W is the weight of each station (calculated by using Lv's scheme to determine the residual effect), TB is the calculated brightness temperature for each station and n is the number of stations. A single value of the TB representing the whole network is calculated based on these weights.

The description of weight functions as proposed by (Lv et al., 2016) is further described in **Appendix C** to show the theory and calculation of each stations weight function.

3.3. SMAP L1C Brightness Temperature

The SMAP satellite sensor is placed in a sun-synchronous 6:00 am to 6:00 pm orbit based on scientific concerns pertinent for the L2_SM_P product. The SMAP sensor radiometry physics are described in the ATBD handbook. The main sources of error that the SMAP scientific development team predict are the Faraday rotation, atmospheric effects, and low-level RFI effects. At L-Band frequencies, the atmosphere is fundamentally transparent, with the atmospheric transmissivity $\tau_{atm} \approx 1$. The cosmic background (T_{sky}) is approximately 2.7 K. The emissions from the atmosphere are very small. SMAP L1B_TB accounts for this atmospheric contributions (McNairn et al., 2015; Neill et al., 2012a; Panciera, Walker, Jackson, Gray, Tanase, Ryu, Moneris, Yardley, Rüdiger, et al., 2014).

Faraday rotation occurs when the polarization direction of an electromagnetic wave revolves as the wave propagates through the ionosphere in presence of the Earth's static magnetic field. This increases the polarisation as a square of wavelength. If uncorrected, the SMAP polarized (H and V) radiometer measurements will contain errors that translate to soil moisture error. Faraday rotation varies greatly during the day, reaching a maximum during the afternoon and a minimum in the pre-dawn hours. By using TB observations acquired near 6:00 am local solar time as the primary input to the L2_SM_P product, the adverse impacts of Faraday rotation are minimized. Faraday rotation correction to SMAP TB is described in the L1B_TB ATBD. At 6:00 am, the vertical profiles of soil temperature and soil dielectric properties are likely to be uniform than at other times of the day. This early morning condition will minimize the difference between canopy and soil temperatures and thermal differences between land cover types within a pixel. These factors help to minimize retrieval errors originating from the use of a single effective temperature to represent the near surface soil and canopy temperatures. This same effective temperature can be used as the open water temperature in the water body correction to TB (Yueh, 2015).

SMAP L1C brightness temperature products were downloaded from NSIDC DAAC FTP site as shown in Table 5 below. The datasets provide daily brightness temperature products at different hours. The SMAP L1C brightness temperature files per each measurement instance are contained in HDF5 files which includes different datasets in EASE2 grid. The datasets that are included in the SMAP LIC Brightness temperature file include, cell brightness temperature in the fore and aft looking angles of the satellites for both H, V, 3rd and 4th stokes parameter. This are the most important datasets for the evaluation of the brightness temperature products. Other datasets for each individual HDF5 file include the brightness temperature errors in aft and fore looking H, V, 3rd and 4th stokes parameters. This datasets are important because they will represent the threshold of the errors from the products.

The HDF5 files were visualized using HDFview from HDF group. In order to read the datasets in each LIC file, a matlab code to read hdf5 SDS was developed to retrieve brightness temperature values for the SMAP TBH and TBV for the period of study. Table 9 shows the corresponding SMAP satellite overpass time in Maqu during the study period. The Table indicates that the number of Satellite Overpass in the area during the study period was 37.

The SMAP L1C_TB product is calibrated geolocated and time-ordered L1B_TB brightness temperatures and resampled to the global fixed 36-km EASE2 grid. The L1B_TB data also undergoes correction for Faraday rotation, atmospheric effects, and low-level RFI effects before the process of re-gridding is done. Based on the SMAP ATBD in case of a large RFI for correction, the TB data is flagged accordingly and no soil moisture retrieval is tried.

4. RESULTS

4.1.1. Upscaling of point station data to pixel data

The modelled outputs of the eight stations chosen for the study are upscaled to a single field value to match the SMAP pixel value. Two methods are used for the upscaling method as described in section 3.2. Figure 7 shows the results of the upscaling process for point station effective temperature and the Weight function upscaling effective temperature.

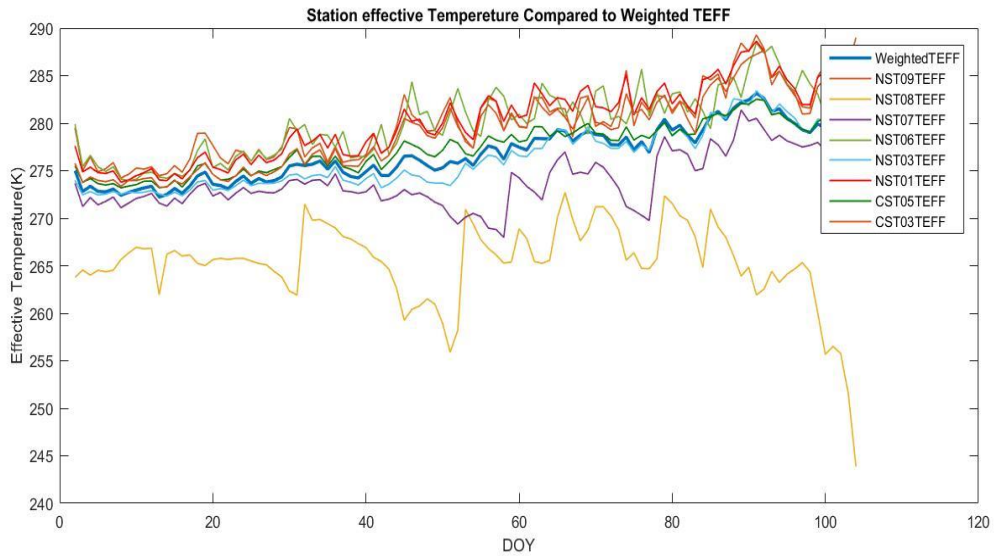


Figure 7: Modelled point station Teff and Weighted Teff

Table 6 below shows the linear norm of residuals when individual stations are compared with the upscaled product using the weight functions and simple upscaling as references. The Lv scheme Effective temperature is used to illustrate the contribution of each station to the overall error budget when it comes to upscaling.

Table 5: Stations error contribution

STATION Name	Norm of residuals (K) (Weight functions upscaling)	Norm of Residuals (K) (Simple average upscaling)	Percentage error contribution (%)
CST03	11.3892	12.4467	9.414675508
CST05	5.4755	6.1173	4.627121606
NST01	10.1321	10.9908	8.313433728
NST03	6.1201	6.8768	5.201606895
NST06	16.9262	17.2008	13.01067355
NST07	18.3875	18.6059	14.07349025
NST08	44.1284	44.1156	33.36901017
NST09	15.0859	15.8514	11.9899883

The results above shows that NST08 has a large error contribution compared to the rest of the station when both the simple average and weight functions are used as references with station modelled effective temperature output. CST05 has the least error residual when matched with the simple average and weight function product. NST08 has an error contribution of about 33.3% while CST05 only contributes 4.6% to

the total error budget. Hence, for the eight stations shown above, CST05 dataset is more representative of the field while NST08 dataset has a poor representation at a field scale. To generate new weights, CST05 will be given a higher weight function value while NST08 will be given the least weight function to reduce the error due to this station.

4.1.2. Comparison of different Effective Temperature schemes

The four main effective temperature schemes used to parameterize effective temperature are the Choudhury, Wigneron, Holmes and Lv scheme. The parameterization of the effective temperature by each scheme is described in the methodology (Figure 3). The different schemes are compared after upscaling the modelled outputs from individual stations. The comparison is done for the simple average and the weight functions upscaling method.

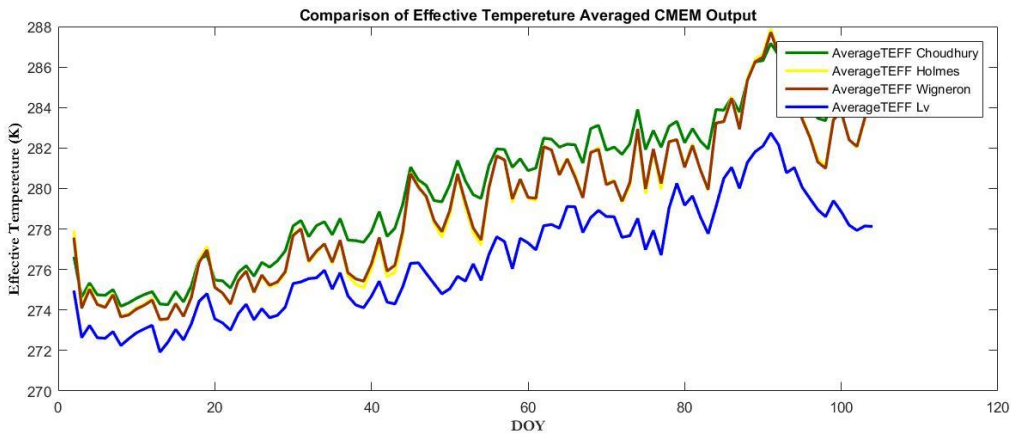


Figure 8: Effective Temperature schemes simulations using simple average upscaling

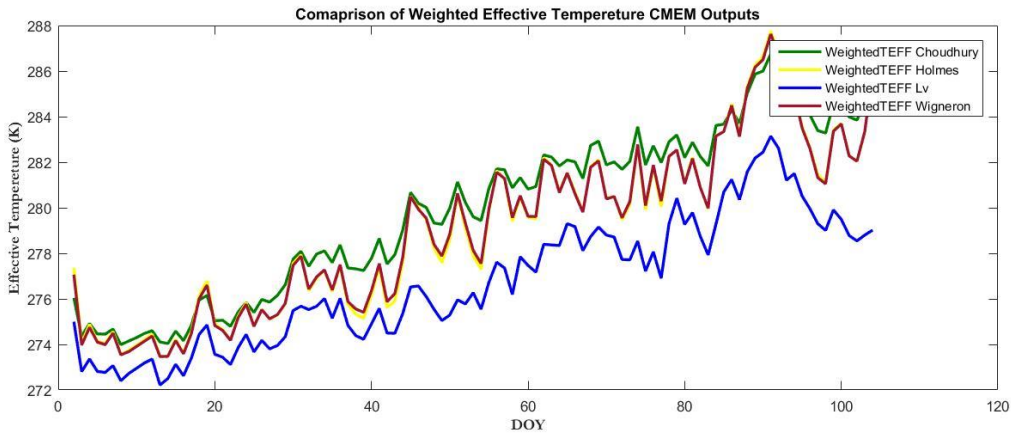


Figure 9: Effective Temperature schemes simulations using weight functions upscaling

The different effective temperature schemes provide different values of modelled effective temperature. Figure 8 shows the results of the four different effective schemes after simple average upscaling of all the stations. The Choudhury scheme produces a higher effective temperature while the Lv scheme produces lower effective temperature values. Holmes and Wigneron result in matches, which have a near perfect shape. The time series above shows that Holmes and Wigneron schemes have a higher simulation compared with Lv scheme. The consistency of the simulations is same for all the two methods of upscaling as shown in Figure 8 and Figure 9.

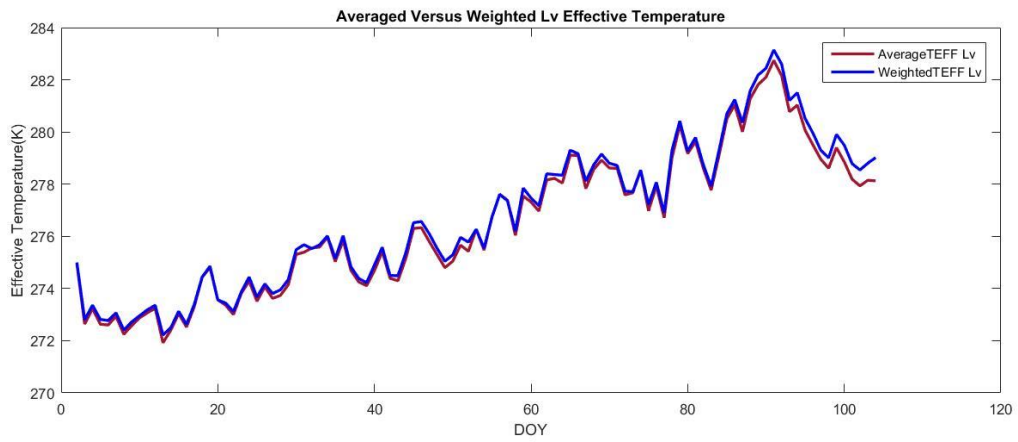


Figure 10: Comparison of simple upscaling versus Lv Weight functions upscaling

The weighted functions upscaling method is derived from the Lv scheme for effective temperature parameterization. Comparing the weighted function method to the simple average method on the Lv parameterized effective temperature, the simple average method results in slightly higher effective temperature compared to the weighted function. Figure 10 above shows the comparison between the two upscaling methods when applied on the Lv modelled Effective temperature scheme.

4.1.3. Modelled TBH and TBV outputs based on the different effective temperature schemes

The effect of different effective temperature schemes can be clearly seen in the Brightness temperature outputs. The modelled brightness temperature based on the different effective temperature schemes and upscaled using the Lv derived weight functions is shown in Figure 11 and Figure 12 for H and V polarization for respectively. The Lv scheme results in higher modelled outputs in both the H and V polarization compared to the other schemes. Wigneron, Choudhury and Holmes result in brightness temperatures in H and V polarisations, which are far low, compared to the Lv scheme.

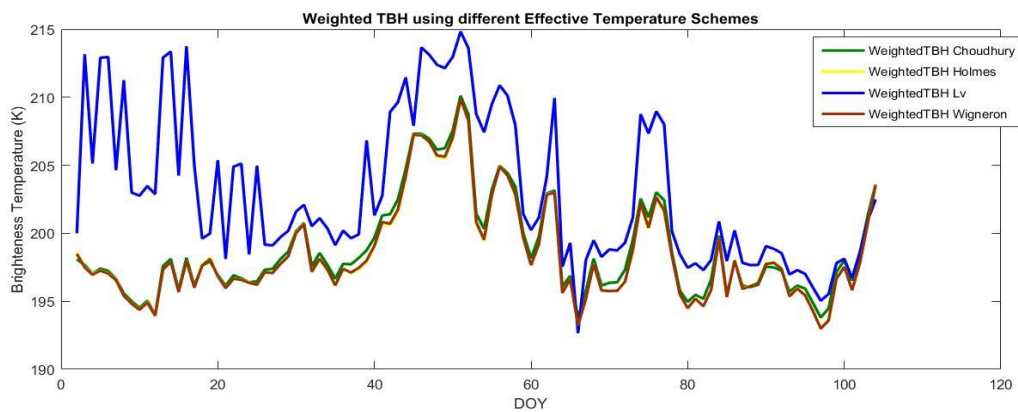


Figure 11: Effective Temperature schemes TBH outputs using weighted function upscaling

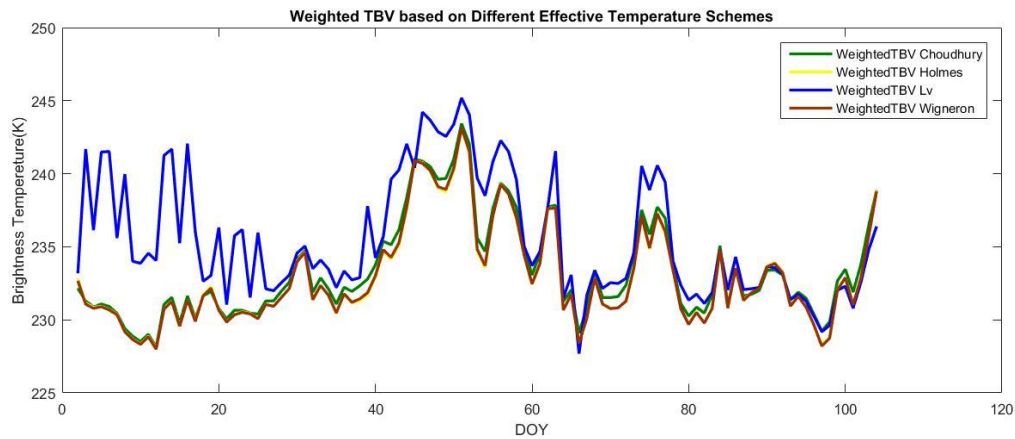


Figure 12: Effective Temperature schemes TBV outputs using Lv Weight functions upscaling

The weight functions and Simple averaged H and V are compared in Figure 13 below for the Lv scheme. Based on this comparison, it is clear that simple average upscaling results in higher brightness temperature for both the H and V polarisations. The weighted functions upscaling provides a lower modelled estimate of the brightness temperature in both H and V compared to the simple average upscaling of the stations.

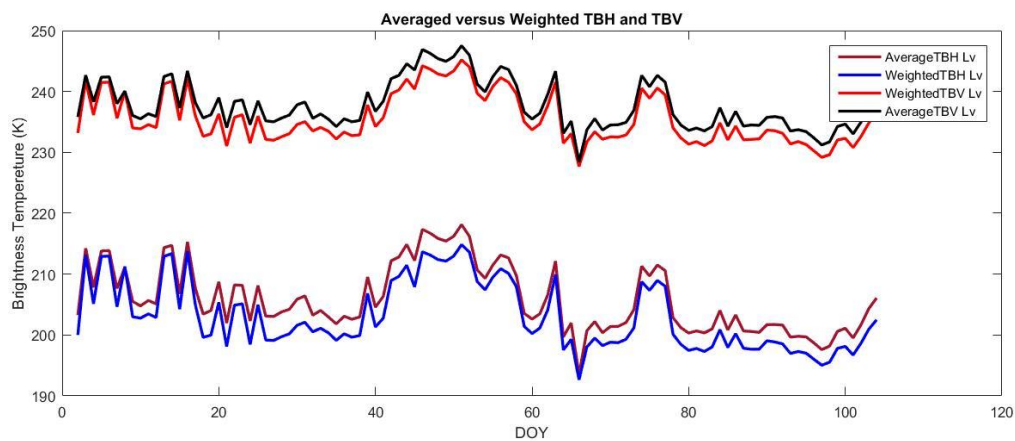


Figure 13: Lv scheme TBH using different upscaling approaches

4.2. Matchup between CMEM and SMAP Brightness Temperature

The SMAP TBV and TBH pixels are averaged to provide a single pixel value which are then compared to the averaged modelled output. For the period between 2015-4-1 to 2015-7-1, the SMAP satellite had 37 overpass over the Maqu network. The comparison is done between the 37 instances when the satellite passes over the network. The assumption for this study is that the satellite overpass is at 6am in the morning when the satellite is in the ascending and descending orbit.

Figure 14 and Figure 15 show the relationship between modelled brightness temperatures in horizontal polarisation based on the different effective temperature scheme. The comparison is done for the two methods of upscaling. In both instances, SMAP TBH is higher compared to the modelled outputs for both instances. The Lv scheme has a higher modelled TBH compared to the other effective temperature scheme when compared with SMAP TBH for both instances of upscaling methods. The general trend for the period of study over the three months shows some correlation but there is less correlation when point-to-point comparison is done between SMAP TBH and the modelled outputs for all the instances.

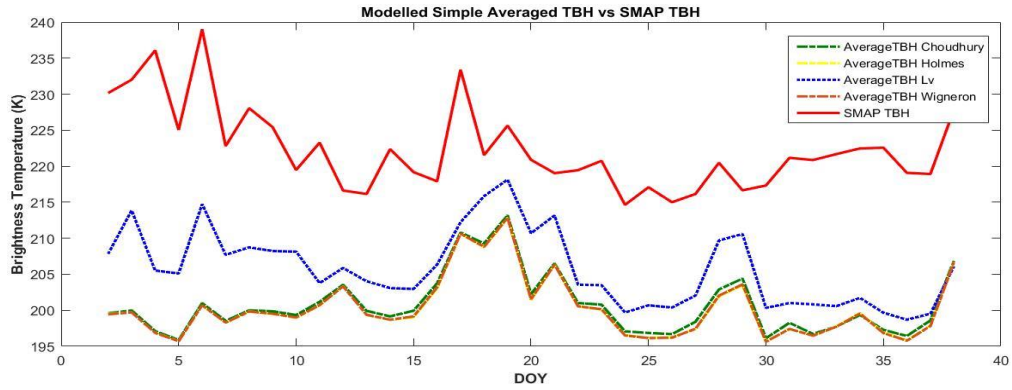


Figure 14: SMAP versus simple average modelled TBH

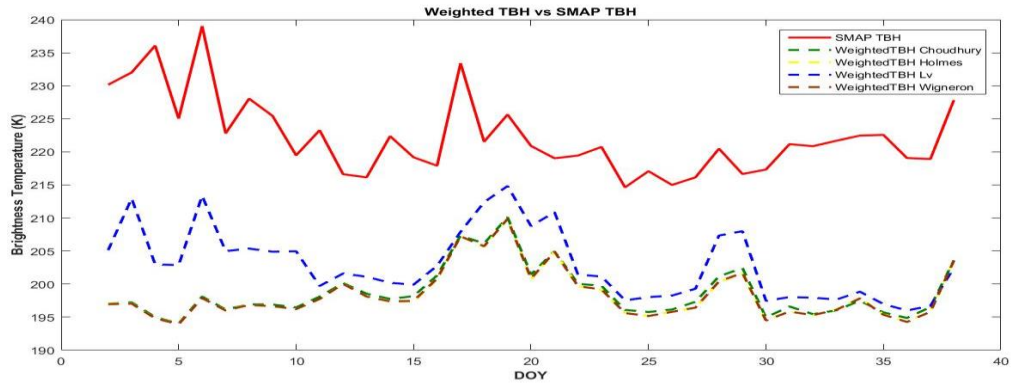


Figure 15: SMAP versus weight function upscaling modelled TBH

Figure 16 and Figure 17 show the comparison between modelled TBV outputs upscaled by both upscaling methods for the different effective temperature schemes with SMAP TBV. Based on these results, there is some correlation between SMAP TBV and the general network output. When using the simple average upscaling, higher values of output TB are observed in the Lv scheme. However, a combination of the Lv scheme and the weighted function shows less over-estimation when compared to SMAP TBV. For the comparison between the modelled TBV from the other effective temperature schemes outputs, underestimation is clearly seen at the beginning and at the end of the study period when compared to SMAP TBV.

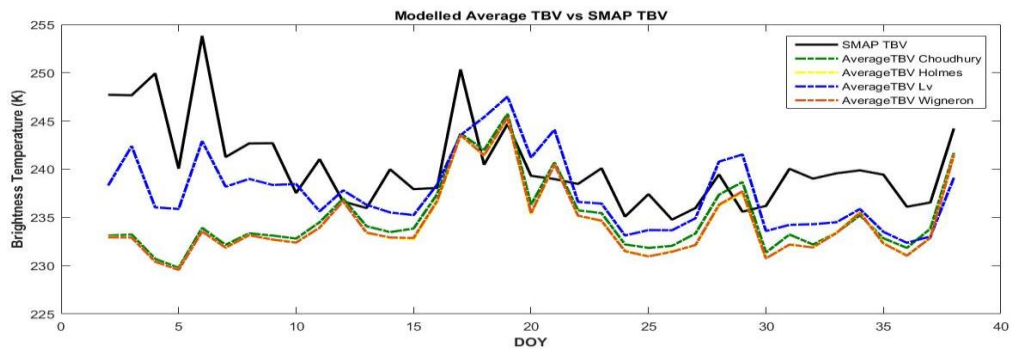


Figure 16: SMAP versus simple average upscaling modelled TBV

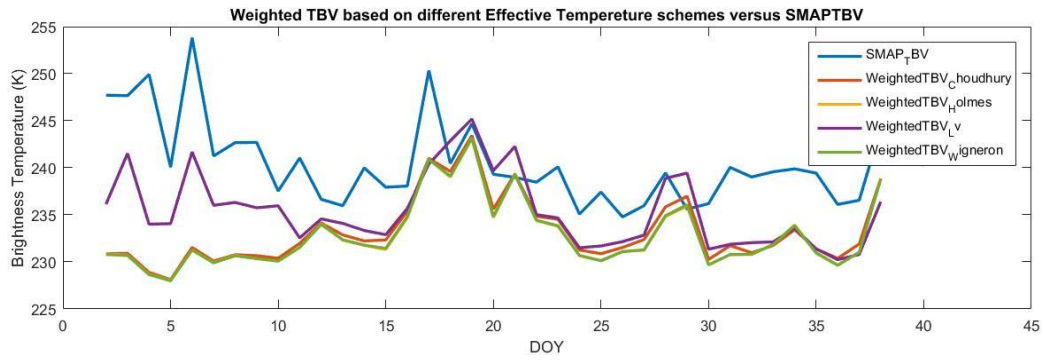


Figure 17: SMAP versus weight function upscaling modelled TBV

Figure 18 is a summary of the Lv scheme weighted function model outputs for TBH and TBV with SMAP TBH and TBV. The Lv scheme models brightness temperature, which is nearly as high as the SMAP in the V polarisation, while in the H polarisation, the modelled output is less compared to the SMAP output. The simple average upscaling has higher modelled outputs compared to the weight functions upscaling when compared to the SMAP observations.

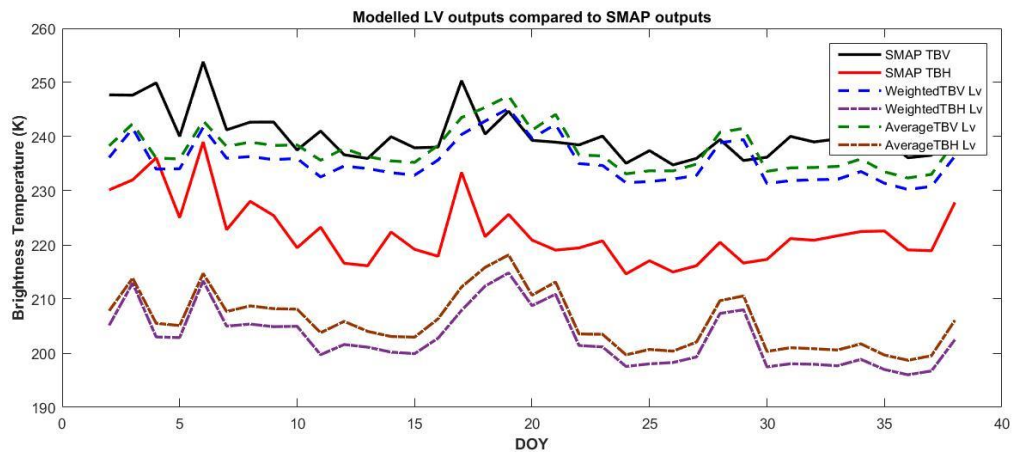


Figure 18: Lv Scheme TBH and TBV with SMAP using different upscaling approaches

5. DISCUSSIONS

The correlation statistics of the validation of SMAP TB with CMEM weighted TB are shown in the scatter plots in Appendix E and F. Table 6 and Table 7 summarises the statistical analysis between the SMAP TB products and the CMEM model upscaled TB products.

Table 6: Statistical analysis of H-polarised modelled versus SMAP TBH

Brightness Temperature Horizontal Pol	SMAP	Lv		Choudhury		Wigner		Holmes	
		Weight	Avg	Weight	Avg	Weight	Avg	Weight	Avg
Bias(K)		19.33	16.53	23.63	21.62	23.97	22.11	23.98	22.06
Mean(K)	222.32	200.56	205.79	198.70	200.70	198.35	200.01	198.35	200.26
Correlation	1.0	0.25	0.25	0.01	0.04	0.02	0.05	0.02	0.06
RMSE		20.10	17.42	24.52	22.54	24.83	9.24	24.82	22.93

Table 7: Statistical analysis of V-polarised modelled versus SMAP TBV

Brightness Temperature Vertical Pol	SMAP	Lv		Choudhury		Wigner		Holmes	
		Weight	Avg	Weight	Avg	Weight	Avg	Weight	Avg
Bias (K)		4.97	2.99	7.18	5.44	7.61	5.97	7.61	5.98
Mean (K)	240.39	235.43	237.43	233.21	234.95	232.78	234.42	232.78	234.42
Correlation	1.0	0.27	0.26	0.01	0.04	0.02	0.06	0.03	0.06
RMSE		6.46	4.99	8.96	7.51	9.24	7.84	9.23	7.61

Table 6 and Table 7 above show that the Lv scheme has a better bias compared to the other scheme in both the H and V polarisations when referenced to SMAP satellite observations. This trend is observed for both the Simple average and Weight functions upscaling. In both methods, a higher correlation is observed when compared to the other methods. The correlation coefficient indicates the similarities in patterns between the modelled CMEM output and the SMAP satellite observations. When we consider simple average upscaling which shows higher correlation compared to the weight functions upscaling, in the H polarization, Lv has a correlation of 0.25 compared to Choudhury (0.04), Wigner (0.05) and Holmes (0.06). In the V polarization, Lv has a correlation of 0.26 compared to Choudhury (0.04), Wigner (0.06) and Holmes (0.06). The Lv scheme modelled brightness temperature has a better correlation coefficient (R) with the SMAP observation in both the H and V polarization.

It is important to note that in the H polarization, the correlation of the modelled Tb is same when using simple average upscaling (0.25) and the weight functions upscaling (0.25) correlation. However, in the V

polarization, a very slight difference in terms of correlations is observed where simple average upscaling correlation (0.26) is slightly lower compared to the weight functions upscaling correlation (0.27).

The RMSE for Lv is also better compared to those of the other schemes. When the Lv scheme is used the RMSE reduces considerably compared to the other scheme. In the H polarization, the RMSE error reduces from as high as 24.83 for Wigner to 20.10K while in the V polarization, it reduces from as high as 9.24K to 6.46K. This is an indication that using the Lv scheme is optimal compared to the other schemes on a general scale. Applying the simple average upscaling improves the RMSE in both the H and V polarisations when compared to the weight function upscaling for Lv scheme and the other effective schemes.

This RMSE is high and this may be due to several assumptions made in the study. The Assumption that the vegetation in the network is C3 may be the biggest contributing factor to the large error as shown in Figure 19. Assuming the vegetation in the network to be C4 grassland improves this errors as shown below. This is shown in Figure 20, where C4 grassland increases the modelled brightness temperature to the SMAP pixel level in both the H and V polarization.

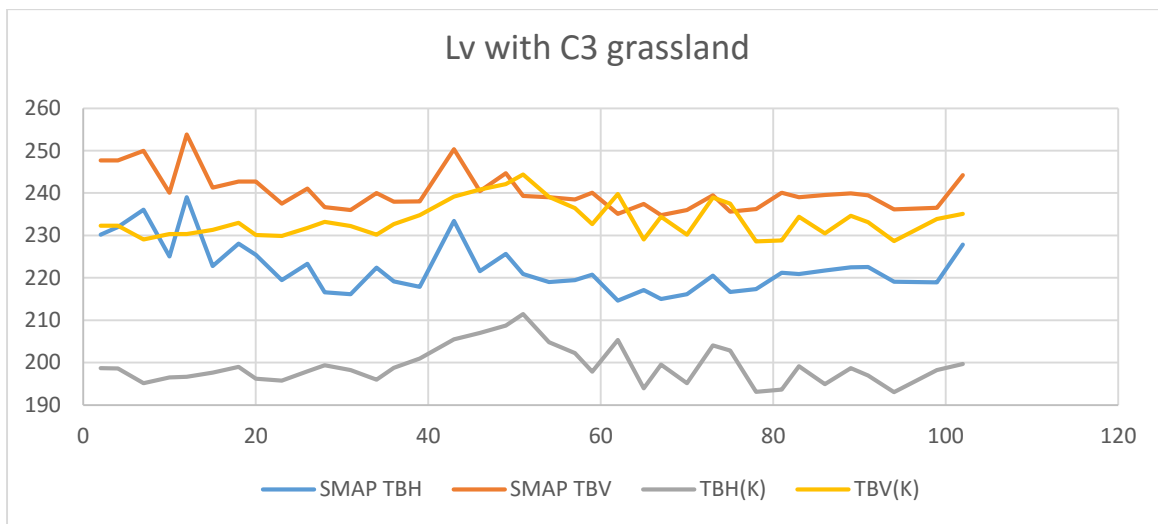


Figure 19: CST05 comparison with SMAP using the Lv scheme in the described study.

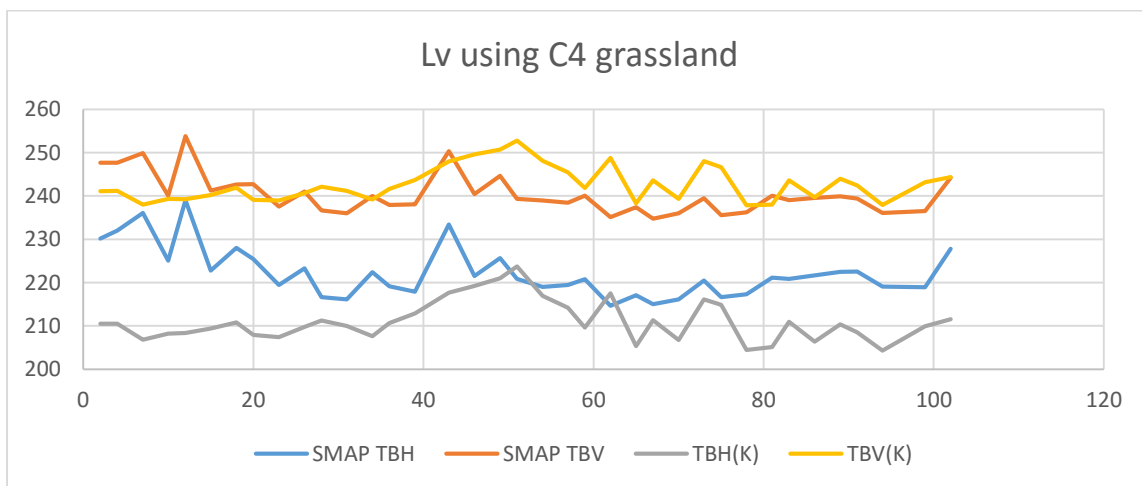


Figure 20: CST05 comparison with SMAP using the Lv scheme in using C4 grassland.

The best method for upscaling as shown by the results and discussions above is the use of simple average upscaling. However, the differences between weight functions approach and the simple upscaling is very minimal for all the different effective temperature schemes. This shows that the use of weight functions to upscale point soil data as described by Lv et al 2016, is a viable option.

In describing the uncertainties in the Maqu network, the Lv scheme is the best option for the parameterization of effective temperature when considering the bias, RMSE and correlation with SMAP TB products. The Lv effective temperature scheme computes brightness temperature that has a better correlation with the SMAP satellite observation when compared to the other schemes can be attributed to the concept of approximating the C parameter by utilizing soil moisture, soil temperature from multiple layers (Lv et al., 2014). The Lv scheme proves that it can be used to calculate effective temperature for the SMAP satellite radiometer.

The main sources of uncertainties between the CMEM modelled outputs and the SMAP observations may be due to the other modules of the CMEM model. Holmes (2006) suggests that vegetation has a huge influence on the dynamic range of modelled brightness temperature. The CMEM setup used in this research assumes a static vegetation to parameterise the vegetation opacity model (Schwank et al., 2012). This may contribute to the high errors in terms of correlation between CMEM and SMAP observation. The model setup uses the ECOCLIMAP-ECMWF derived inputs. TESSEL and HTESSEL are two options that can be used to show the sensitivity of CMEM to vegetation effects. According to Holmes (2006), vegetation data is a main source of this uncertainty because of the assumption by CMEM that the vegetation is static and not dynamic. By improving the accuracy of the vegetation layer, it is possible to reduce the systematic errors in the CMEM comparisons with satellite observations.

Drusch (2007) suggests that combination of different data sets in an advanced investigation scheme is a challenge due to the little knowledge on the spatial and temporal unpredictability of systematic and random errors in both satellite observations and the model. In this study, it is important to note that the SMAP satellite has been operational for less than one year and science are still working on calibrating and validating the satellite observation. While the SMAP L1C algorithm shows how random errors in the observations can be reduced, errors due to Faraday rotation and RFI contamination can be an issue. The Tibetan plateau is notorious for RFI contamination as shown by several studies such as (Zeng et al., 2015), Mitigation of RFI contamination in the Tibetan plateau has been proposed by (Zeng et al., 2015, Su et al., 2011 and Njoku et al., 2003). Figure 21 shows the areas that have high RFI contamination based on the SMOS product. The Tibetan plateau is one of the area and for recent SMOS evaluation; the threshold set has resulted in lack of TB observations in the region.

The SMAP satellite employs dynamic surface temperature data from GMAO GEOS-5 model as part of the functional processing of the SMAP passive soil moisture product (West, 2014). GMAO baseline computation of brightness temperature exploits the average surface temperature and the GMAO layer 1 soil temperature at 10 cm. This designates a homogenous soil temperature profile between the surface and the deepest sensing depth. This assumption cannot hold for arid and semi-arid areas or areas with high seasonal variability like the Tibetan Plateau (Yueh, 2015). A more sophisticated method has to be applied in order to handle the soil profiles with non-uniform temperatures. In order to address this problem, the Lv scheme is the most effective considering the two-layer approach, which estimates effective temperature based on soil moisture, soil temperature, sensing depth and wavelength of the sensor (Yueh, 2015).

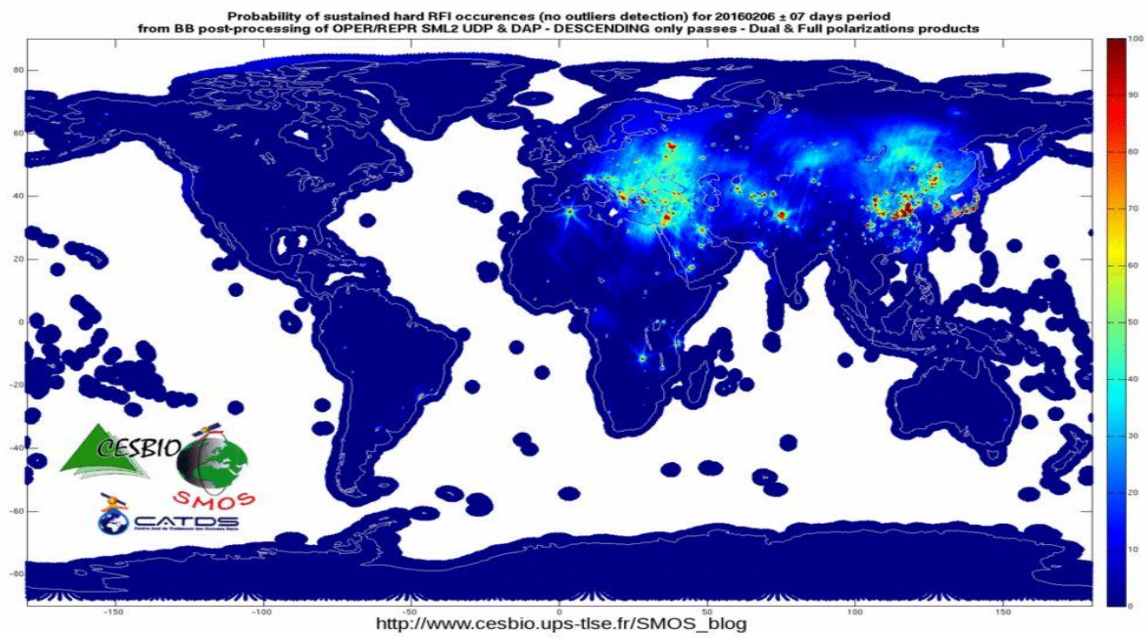


Figure 21: Latest RFI contaminated areas map from SMOS

6. CONCLUSION AND RECOMMENDATIONS

The Tibetan plateau is a unique hydroclimate that influences land atmosphere interactions on the Asian subcontinent. This is because of the high elevation (about 4000m.a.s.l) of the area and its characterisation by the South Asian Monsoon. Identifying brightness temperature and related uncertainties in the region provides a deeper understanding of the land surface interactions in the region. Modelling in-situ measurements and comparing them with radiometer observations on board satellites such as the SMAP and SMOS missions, allows us to understand and quantify the sources of uncertainties in this region.

This study has shown that

- Using Soil moisture and soil temperature in-situ measurements from the Maqu SMST network, makes it possible to model brightness temperature through different parameterisations in the CMEM model. The CMEM model simulations need soil moisture and soil temperature together with other ancillary data such as leaf area index, skin temperature, air temperature at 2 metres and soil texture information.
- Effective temperature schemes are important in parameterisation of modelling brightness temperature. The two-layer approach used in the Lv scheme makes it a more effective scheme in ensuring that contributions by the deepest layers are included in the modelling of brightness temperature. The ability of the Lv scheme to model brightness temperature that shows a higher correlation with the SMAP brightness temperature outputs in the Maqu network proves that while the instrument only snaps the moisture content of the top soil layer, this contribution is based on the all contributions from the deepest layers of the soil storage layer.
- The simple average upscaling has less residuals when compared to the weight functions as proposed by Lv. The upscaling analysis also shows that NST08 (33.3%) has a larger contribution of errors to the field value while CST05 (4.6%) is more representative of the network average and can be used to represent the field average.
- In the H polarization, the RMSE error reduces from as high as 24.83 for Wigneron to 20.10K for Lv scheme while in the V polarization, from as high as 9.24K for Wigneron to 6.46K for Lv scheme. Applying the simple average upscaling improves the RMSE in both the H and V polarisations when compared to the weight function upscaling for Lv scheme and the other effective schemes. The error in the H polarization is high and it can be associated with the assumption of the study area having C3 grassland instead of C4 grassland. Vegetation has a higher effect on the emission of this layers.
- LV effective temperature scheme computes brightness temperature that has a better correlation with the SMAP satellite observation when compared to the other schemes. In the H polarisation, Lv has a correlation coefficient of 0.25 compared to Choudhury (0.04), Wigneron (0.05) and Holmes (0.06). In the V polarization, Lv has a correlation of 0.26 compared to Choudhury (0.04), Wigneron (0.06) and Holmes (0.06).

This research recommends that further studies be carried using the Lv scheme with different parameterisations for the other different modules of the CMEM. This will help understand the sources of errors in CMEM modelling when compared to SMAP. The installation of an ELBARA sensor at the network is important in helping calibrate and validate satellite brightness temperature for this region. A

study that will consider the outputs of the ELBARA radiometer will help in quantification of uncertainties associated with brightness temperature in the network.

LIST OF REFERENCES

- Behari, J. (2005a). *Microwave dielectric behavior of wet soils*. Springer/Anamaya (3rd ed., Vol. 8). New Delhi, India: Springer. <http://doi.org/10.1016/j.geoderma.2005.08.001>
- Behari, J. (2005b). *Microwave dielectric behaviour of wet soils*. *Polar Record* (Vol. 25). <http://doi.org/10.1017/S0032247400010123>
- Choudhury, B. J., Schmutge, T. J., Chang, a., & Newton, R. W. (1979). Effect of surface roughness on the microwave emission from soils. *Journal of Geophysical Research*, 84(C9), 5699. <http://doi.org/10.1029/JC084iC09p05699>
- De Lannoy, G. J. M., Pauwels, V. R. N., Houser, P. R., Gish, T., & Verhoest, N. E. C. (2007). Representativeness of point soil moisture observations, upscaling and assimilation. *LAHS-AISH Publication*, (313), 249–257. Retrieved from <http://www.scopus.com/inward/record.url?eid=2-s2.0-55749102458&partnerID=tZOtx3y1>
- de Rosnay, P., Drusch, M., & Sabater, J. M. (2009). Contract Report to the European Space Agency Milestone 1 Tech Note - Part 1 : SMOS Global Surface Emission Model. *Progressive Report for ESA Contract*, 1(1), 1–20. Retrieved from https://software.ecmwf.int/wiki/display/LDAS/CMEM+Documentation?preview=/29328373/29525142/ESA_11640_derosnay_MS1TNPI_2009.pdf
- Drusch, M. (2007). Initializing numerical weather prediction models with satellite-derived surface soil moisture: Data assimilation experiments with ECMWF's integrated forecast system and the TMI soil moisture data set. *Journal of Geophysical Research Atmospheres*, 112(3), 1–14. <http://doi.org/10.1029/2006JD007478>
- EOportal Directory. (2014). SMAP (Soil Moisture Active/Passive) Mission. Retrieved from <https://directory.eoportal.org/web/eoportal/satellite-missions/1/lageos>
- Fennessy, M. J., & Shukla, J. (1999). Impact of initial soil wetness on seasonal atmospheric prediction. *Journal of Climate*, 12(11), 3167–3180. [http://doi.org/10.1175/1520-0442\(1999\)012<3167:IOISWO>2.0.CO;2](http://doi.org/10.1175/1520-0442(1999)012<3167:IOISWO>2.0.CO;2)
- Holmes, T. R. H. (2006). SMOS Community Microwave Emission Model (SMOS-CMEM), (December).
- Jackson, T., Colliander, A., Kimball, J., Reichle, R., Crow, W., Entekhabi, D., & Neill, P. O. (2012). Science Data Calibration and Validation Plan.
- Jackson, T. J., & Schmutge, T. J. (1991). Vegetation effects on the microwave emission of soils. *Remote Sensing of Environment*, 36(3), 203–212. [http://doi.org/10.1016/0034-4257\(91\)90057-D](http://doi.org/10.1016/0034-4257(91)90057-D)
- Johnson, J. (2012). Soil Moisture Active Passive (SMAP) Algorithm Theoretical Basis Document SMAP L2 & L3 Radar Soil Moisture (Active) Data Products.
- Kerr, Y. H., Waldteufel, P., Wigneron, J. P., Martinuzzi, J., Font, J., & Berger, M. (2001). Soil moisture retrieval from space: the Soil Moisture and Ocean Salinity (SMOS) mission. *Geoscience and Remote Sensing, IEEE Transactions on*, 39(8), 1729–1735.
- Koster, R. D., & Suarez, M. J. (1999). A simple framework for examining the interannual variability of land surface moisture fluxes. *Journal of Climate*, 12(7), 1911–1917. [http://doi.org/10.1175/1520-0442\(1999\)012<1911:ASFFET>2.0.CO;2](http://doi.org/10.1175/1520-0442(1999)012<1911:ASFFET>2.0.CO;2)
- Laboratories, E. S. (2007). SMOS level 2 Processor for Soil Moisture Algorithm Theoretical Based Document (ATBD) Document status Sheet, (2).
- Lv, S., Wen, J., Zeng, Y., Tian, H., & Su, Z. (2014). An improved two-layer algorithm for estimating effective soil temperature in microwave radiometry using in situ temperature and soil moisture measurements. *Remote Sensing of Environment*, 152, 356–363. <http://doi.org/10.1016/j.rse.2014.07.007>
- Lv, S., Zeng, Y., WEN, J., ZHENG, D., & SU, Z. (2016). Determination of the Optimal Mounting Depth for Calculating Soil Effective Temperature at L-band: Maqu Case. *Remote Sensing*.
- Magagi, R., Berg, A. A., Goita, K., Belair, S., Jackson, T. J., Toth, B., ... Merzouki, A. (2013). Canadian experiment for soil moisture in 2010 (CanEx-SM10): Overview and preliminary results. *IEEE Transactions on Geoscience and Remote Sensing*, 51(1), 347–363. <http://doi.org/10.1109/TGRS.2012.2198920>
- McNairn, H., Jackson, T. J., Wiseman, G., Belair, S., Berg, A., Bullock, P., ... Hosseini, M. (2015). The soil moisture active passive validation experiment 2012 (SMAPVEX12): Prelaunch calibration and validation of the SMAP soil moisture algorithms. *IEEE Transactions on Geoscience and Remote Sensing*, 53(5), 2784–2801. <http://doi.org/10.1109/TGRS.2014.2364913>

- Miernecki, M., Wigneron, J.-P., Lopez-Baeza, E., Kerr, Y., De Jeu, R., De Lannoy, G. J. M., ... Richaume, P. (2014). Comparison of SMOS and SMAP soil moisture retrieval approaches using tower-based radiometer data over a vineyard field. *Remote Sensing of Environment*, 154, 89–101. <http://doi.org/10.1016/j.rse.2014.08.002>
- Neill, P. O., Chan, S., Njoku, E., Jackson, T. J., & Bindlish, R. (2012a). *Soil Moisture Active Passive (SMAP) Algorithm Theoretical Basis Document (ATBD) SMAP Level 2 & 3 Soil Moisture (Passive)* (Vol. A). Santa Barbara, California: Jet Propulsion Laboratory, California Institute of Technology. Retrieved from <http://smap.jpl.nasa.gov/science/dataproducts/ATBD/>
- Neill, P. O., Chan, S., Njoku, E., Jackson, T. J., & Bindlish, R. (2012b). Soil Moisture Active Passive (SMAP) Algorithm Theoretical Basis Document (ATBD) SMAP Level 2 & 3 Soil Moisture (Passive), 1–76. Retrieved from <http://smap.jpl.nasa.gov/science/dataproducts/ATBD/>
- Newton, R. W., Heilman, J. L., & Van Bavel, C. H. M. (1983). Integrating passive microwave measurements with a soil moisture/heat flow model. *Agricultural Water Management*, 7(1-3), 379–389. [http://doi.org/10.1016/0378-3774\(83\)90097-5](http://doi.org/10.1016/0378-3774(83)90097-5)
- Njoku, E. G., & Entekhabi, D. (1996). Passive Microwave Remote Sensing of Soil Moisture, 46.
- Njoku, E. G., Jackson, T. J., Lakshmi, V., Chan, T. K., & Nghiem, S. V. (2003). Soil moisture retrieval from AMSR-E. *IEEE Transactions on Geoscience and Remote Sensing*, 41(2 PART 1), 215–228. <http://doi.org/10.1109/TGRS.2002.808243>
- Panciera, R., Walker, J. P., Jackson, T. J., Gray, D. A., Tanase, M. A., Ryu, D., ... Hacker, J. M. (2014). The soil moisture active passive experiments (SMAPEX): Toward soil moisture retrieval from the SMAP mission. *IEEE Transactions on Geoscience and Remote Sensing*, 52(1), 490–507. <http://doi.org/10.1109/TGRS.2013.2241774>
- Panciera, R., Walker, J. P., Jackson, T. J., Gray, D. a., Tanase, M. a., Ryu, D., ... Hacker, J. M. (2014). The soil moisture active passive experiments (SMAPEX): Toward soil moisture retrieval from the SMAP mission. *IEEE Transactions on Geoscience and Remote Sensing*, 52(1), 490–507. <http://doi.org/10.1109/TGRS.2013.2241774>
- Parrens, M., Calvet, J.-C., de Rosnay, P., & Decharme, B. (2014). Benchmarking of L-band soil microwave emission models. *Remote Sensing of Environment*, 140, 407–419. <http://doi.org/10.1016/j.rse.2013.09.017>
- Piepmeyer, J., Mohammed, P., Amici, G. De, Kim, E., Peng, J., & Ruf, C. (2014). *Soil Moisture Active Passive (SMAP) Algorithm Theoretical Basis Document (ATBD) SMAP Calibrated, Time-Ordered Brightness Temperatures L1B - TB Data Product* (Vol. A). Santa Barbara, California: Jet Propulsion Laboratory, California Institute of Technology.
- Rosnay, P. De, Drusch, M., Boone, A., Balsamo, G., Decharme, B., Harris, P., ... De Rosnay, P. (2008). The Amma Land Surface Model intercomparison Experiment coupled to the Community Microwave Emission Model: ALMIP-MEM. *Journal of Geophysical Research*, 114(July), D05108. <http://doi.org/doi:10.1029/2008JD010724>
- Schmugge, T. J., O'Neill, P. E., & Wang, J. R. (1986). Passive Microwave Soil Moisture Research. *IEEE Transactions on Geoscience and Remote Sensing*, GE-24(1), 12–22. <http://doi.org/10.1109/TGRS.1986.289585>
- Schwank, M., Wigneron, J. P., López-Baeza, E., Völsch, I., Mätzler, C., & Kerr, Y. H. (2012). L-band radiative properties of vine vegetation at the MELBEX III SMOS cal/val site. *IEEE Transactions on Geoscience and Remote Sensing*, 50(5 PART 1), 1587–1601. <http://doi.org/10.1109/TGRS.2012.2184126>
- Simmer, C. (1999). Contribution of microwave remote sensing from satellites to studies on the Earth energy budget and the hydrological cycle. *Advances in Space Research*, 24(7), 897–905. [http://doi.org/10.1016/S0273-1177\(99\)00365-8](http://doi.org/10.1016/S0273-1177(99)00365-8)
- Su, Z., Wen, J., Dente, L., Van Der Velde, R., Wang, L., Ma, Y., ... Hu, Z. (2011). The tibetan plateau observatory of plateau scale soil moisture and soil temperature (Tibet-Obs) for quantifying uncertainties in coarse resolution satellite and model products. *Hydrology and Earth System Sciences*, 15(7), 2303–2316. <http://doi.org/10.5194/hess-15-2303-2011>
- Wang, J.R. and Choudhry, B. J. (1981). Remote sensing of soil moisture content over bare field at 1.4 GHz frequency. *J. Geophys. Res*, 86, 5277–5282.
- Wegmüller, U., & Mätzler, C. (1999). Rough bare soil reflectivity model. *IEEE Transactions on Geoscience and Remote Sensing*, 37(3 I), 1391–1395. <http://doi.org/10.1109/36.763303>
- West, R. (2014). Soil Moisture Active and Passive Mission (SMAP) Algorithm Theoretical Basis Document

(ATBD).

- Wigneron, J. P., Kerr, Y., Waldteufel, P., Saleh, K., Escorihuela, M. J., Richaume, P., ... Schwank, M. (2007). L-band Microwave Emission of the Biosphere (L-MEB) Model: Description and calibration against experimental data sets over crop fields. *Remote Sensing of Environment*, 107(4), 639–655. <http://doi.org/10.1016/j.rse.2006.10.014>
- Wigneron, J.-P., Laguerre, L., & Kerr, Y. H. (2001). A simple parameterization of the L-band microwave emission from rough agricultural soils. *IEEE Transactions on Geoscience and Remote Sensing*, 39(8), 1697–1707. <http://doi.org/10.1109/36.942548>
- Wilheit, T. T. (1978). Radiative Transfer in a Plane Stratified Dielectric. *IEEE Transactions on Geoscience Electronics*, 16(2), 138–143. <http://doi.org/10.1109/TGE.1978.294577>
- Yueh, S. (2015). Soil Moisture Active Passive (SMAP) Project Calibration and Validation for the L2 / 3 _ SM _ P Beta-Release Data Products Version 2.
- Zeng, J., Li, Z., Chen, Q., Bi, H., Qiu, J., & Zou, P. (2015). Evaluation of remotely sensed and reanalysis soil moisture products over the Tibetan Plateau using in-situ observations. *Remote Sensing of Environment*, 163, 91–110. <http://doi.org/10.1016/j.rse.2015.03.008>
- Zheng, D. (2015). *Water and Heat Exchanges on the Tibetan Plateau Observation and Modeling of the Yellow River Source Region*. Enschede, The Netherlands: University of Twente.

APPENDICES

Appendix A: Maqu network station characteristics

Table 8: Maqu network station information (Su et al., 2011)

Station name(Sensor ID)	Lat/Lon	Elevation (m)	Depth of Sensor below surface	TPG	LC	BD($kg\ m^{-3}$)	STX
CST_1	33°53' /102°08'	3431	5,10,20,40,80	River Valley	Grass	NA	NA
CST_2	33°40' /102°08'	3449	5,10,20,40,80	River Valley	Grass	NA	NA
CST_3	33°54' /101°58'	3507	5,10,20,40,80	Hill valley	Grass	NA	NA
CST_4	33°46' /101°43'	3504	5,10,20,40,80	Hill valley	Wetland grass	NA	NA
CST_5	33°40' /101°53'	3542	5,10,20,40,80	Hill valley	Grass	NA	NA
NST_1	33°53' /102°08'	3431	5,10,20,40,80	River Valley	Grass	0.96	Silt loam
NST_2	33°53' /102°08'	3434	5,10	River Valley	Grass	0.81	Silt loam
NST_3	33°46' /102°08'	3513	5,10	Hill slope	Grass	0.63	Silt loam
NST_4	33°37' /102°03'	3448	5,10	River Valley	Grass	0.26	Silt loam
NST_5	33°38' /102°03'	3476	5,10,20,40	Hill slope	Grass	0.75	Silt loam
NST_6	34°00' /102°16'	3428	5,10,20,40	River Valley	Grass	0.81	Silt loam
NST_7	33°59' /102°21'	3430	5,10	River Valley	Grass	0.58	Silt loam
NST_8	33°58' /102°36'	3473	5,10	Valley	Grass	1.06	Silt loam
NST_9	33°54' /102°33'	3434	5,10	River Valley	Grass	0.91	Sandy loam
NST_10	33°51' /102°34'	3512	5,10,20,40	Hill slope	Grass	1.05	Loam-Silt loam
NST_11	33°41' /102°28'	3442	5,10	River Valley	Wetland grass	0.24	Silt loam
NST_12	33°37' /102°28'	3441	5,10,20,40,80	River Valley	Grass	1.02	Silt loam
NST_13	34°01' /101°56'	3519	5,10,20,40	Valley	Grass	0.67	Silt loam
NST_14	33°55' /102°07'	3432	5,10	River Valley	Grass	0.68	Silt loam
NST_15	33°51' /101°53'	3752	5,10	Hill slope	Grass	0.78	Silt loam

Appendix B: SMAP Satellite Overpass time

Table 9: SMAP Satellite overpass over the Maqu network during the Study period

4/2/2015	23:46:22	-234.43 KM	descending
4/4/2015	23:21:55	307.44 KM	descending
4/7/2015	23:34:19	37.04 KM	descending
4/10/2015	23:46:22	-234.43 KM	descending
4/12/2015	23:21:55	307.44 KM	descending
4/15/2015	23:34:19	37.04 KM	descending
4/18/2015	23:46:22	-234.43 KM	descending
4/20/2015	23:21:55	307.44 KM	descending
4/23/2015	23:34:19	37.04 KM	descending
4/26/2015	23:46:22	-234.43 KM	descending
4/28/2015	23:21:55	307.44 KM	descending
5/1/2015	23:34:19	37.04 KM	descending
5/4/2015	23:46:22	-234.43 KM	descending
5/6/2015	23:21:55	307.44 KM	descending
5/9/2015	23:34:19	37.04 KM	descending
5/13/2015	10:44:43	-208.51 KM	ascending
5/16/2015	10:56:59	63.24 KM	ascending
5/19/2015	11:08:50	362.14 KM	ascending
5/21/2015	10:44:43	-208.51 KM	ascending
5/24/2015	10:56:59	63.24 KM	ascending
5/27/2015	11:08:50	362.14 KM	ascending
5/29/2015	10:44:43	-208.51 KM	ascending
6/1/2015	10:56:59	63.24 KM	ascending
6/4/2015	11:08:50	362.14 KM	ascending
6/6/2015	10:44:43	-208.51 KM	ascending
6/9/2015	10:56:59	63.24 KM	ascending
6/12/2015	11:08:50	362.14 KM	ascending
6/14/2015	10:44:43	-208.51 KM	ascending
6/17/2015	10:56:59	63.24 KM	ascending
6/19/2015	10:31:59	-479.46 KM	ascending
6/20/2015	11:08:50	362.14 KM	ascending
6/22/2015	10:44:43	-208.51 KM	ascending
6/25/2015	10:56:59	63.24 KM	ascending
6/28/2015	11:08:50	362.14 KM	ascending
6/30/2015	10:44:43	-208.51 KM	ascending
7/3/2015	10:56:59	63.24 KM	ascending
7/8/2015	10:44:43	-208.51 KM	ascending
7/11/2015	10:56:59	63.24 KM	ascending

Appendix C: Weight functions based on Lv scheme (Lv et al., 2016)

Background

The physical concept of soil effective temperature T_{eff} is developed to describe the emissive capacity of a soil column. According to the Rayleigh-Jeans approximation, in the microwave domain the emitted energy from the soil is proportional to the thermodynamic temperature. The brightness temperature T_B is expressed as:

$$T_B = eT_{eff} \quad (1)$$

where T_B is the radiation intensity received by the passive microwave sensor fixed near the soil surface or on the satellite platforms while neglecting the attenuation of atmosphere. e is the emissivity that is strongly related to soil moisture. T_{eff} is the effective temperature and is formulated by Wilheit as:

$$T_{eff} = \int_0^\infty T(x) \alpha(x) \exp\left[-\int_0^x \alpha(x') dx'\right] dx \quad (2)$$

where $\alpha(x) = \frac{4\pi}{\lambda} \varepsilon''(x) / 2[\varepsilon'(x)]^2$. Equation (2) states that T_{eff} at the soil surface is a super position of the intensities emitted at various depths within the soil.

An accurate computation of T_{eff} is thus critical for obtaining relevant values of soil emissivity from brightness temperature measurements. It follows that soil moisture can be retrieved from the estimates of soil emissivity. However, the soil moisture and soil temperature profile information is usually limited in a field experiment. The discrete observation points are installed empirically or thought to be continuous with constant vertical intervals. Recently, a new two-layer scheme (hereafter, Lv's scheme) has been derived directly from Equation (2). This is expressed by Lv et al. 2014 as:

$$T_{eff} = T_1(1 - e^{-B_1}) + T_2 e^{-B_1} \quad (3)$$

in which $B_1 = \Delta x \cdot \frac{4\pi}{\lambda} \cdot \frac{\varepsilon''}{2\sqrt{\varepsilon'}}$, a parameter related to wavelength (λ), to soil moisture through the dielectric constant (ε'' is the imaginary part and ε' is the real part), and to sampling depth (Δx). The soil moisture/temperature (SM/ST, hereafter) can be specified using the values obtained from observation networks (e.g. Maqu Network). λ will be a constant for the specific sensors, i.e., $\lambda = 21$ cm for SMOS and SMAP. This leaves the sampling depth (intervals) as only unknown in Equation (3). Equation (3) can be further developed into a complete multi-layer scheme as:

$$T_{eff} = \underbrace{T_1(1 - e^{-B_1})}_{\text{first layer}} + \sum_{i=2}^{n-1} \underbrace{T_i(1 - e^{-B_i})}_{\text{middle layers}} \prod_{j=1}^{i-1} \underbrace{e^{-B_j}}_{\text{attenuation}} + \underbrace{T_n}_{\text{last layer}} \prod_{j=1}^{n-1} \underbrace{e^{-B_j}}_{\text{attenuation}} \quad (4)$$

where the first, second and third part of the right hand side of the equation represent the 1st, *i*th and *n*th layer (e.g. *i*th represents the layers in the middle, while *n*th represents the last layer). When the first layer has been fixed in field sites, the accuracy Equation (3) and (4) can achieve in estimating T_{eff} depends on the determination of sampling depth (intervals) Δx_i (*i* for *i* th layer).

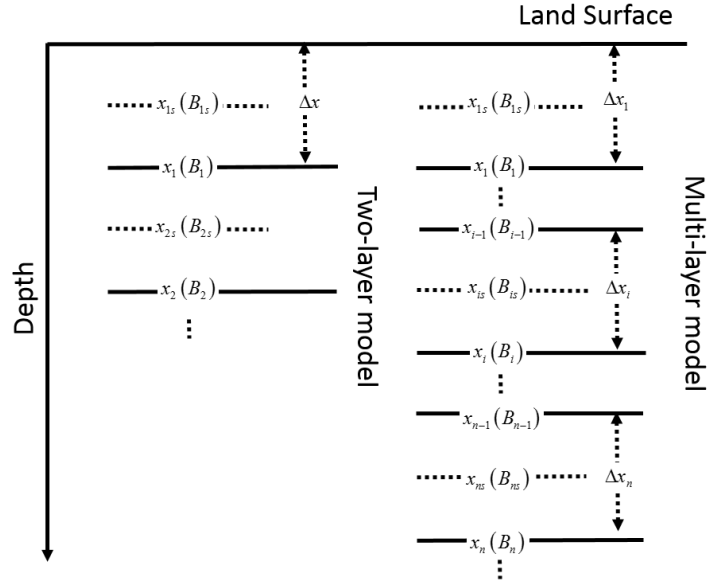


Figure C-1 Schematic of subscripts related to individual soil layers notation

Characteristics of Parameter B

Lv's scheme uses an exponential function to distribute the weight among different layers (see Equation (4)). The only parameter in this scheme is B , which is another form of α in Wilheit's scheme. In order to analyze the characteristics of B , a series of extended concepts are listed in Table C-1.

In fact, Lv's multilayer scheme, which reveals a general form of exponential terms, is more flexible than the two-layer scheme. To achieve either an assessment of the Maqu Network, or a determination of the optimal mounting depth/combination, the multilayer scheme will be deployed. When excluding both the top and bottom layers in the multilayer model, the in-between layers (the i th layer) share a common expression:

$T_i(1 - e^{-B_i}) \prod_{j=1}^{i-1} e^{-B_j}$, with $(1 - e^{-B_i}) \prod_{j=1}^{i-1} e^{-B_j}$ called the weight function (double underline in Equation

(4)). Thus, the weight function could be further divided into two parts: the representative term $(1 - e^{-B_i})$,

which is dealing with B at the i th layer, and the term $\prod_{j=1}^{i-1} e^{-B_j}$, which could be computed with B above

the i th layer. $\prod_{j=1}^{i-1} e^{-B_j}$ determines how much weight from the i th layer can directly contribute to T_{eff}

without any prior knowledge of the $(i+1)$ th layer. In other words, if the $(i+1)$ th layer exists, whatever the soil temperature at the $(i+1)$ th layer is, the soil temperature at the $(i+1)$ th layer has to be multiplied by

$\prod_{j=1}^i e^{-B_j}$. Hence, $\prod_{j=1}^i e^{-B_j}$ can be called the residual (single-underline in Equation 4) of the i th layer. With

these concepts in mind, it is possible to estimate the possible contributions by different layers when calculating T_{eff} .

Table C-1 The mathematical details regarding the concepts mentioned in this study.

Name	The first layer	Middle layers	The deepest layer
B	$B_i = \Delta x_i \cdot \frac{4\pi}{\lambda} \cdot \frac{\varepsilon''}{2\sqrt{\varepsilon'}}$, Δx_i is the physical depth interval. Soil moisture/temperature are from the i th layer as well.		
Residual (R)	e^{-B_1}	$\prod_{j=1}^i e^{-B_j}$	$\prod_{j=1}^n e^{-B_j}$
Weight Function	$1 - e^{-B_1}$	$(1 - e^{-B_i}) \prod_{j=1}^{i-1} e^{-B_j}$	$\prod_{j=1}^{n-1} e^{-B_j}$

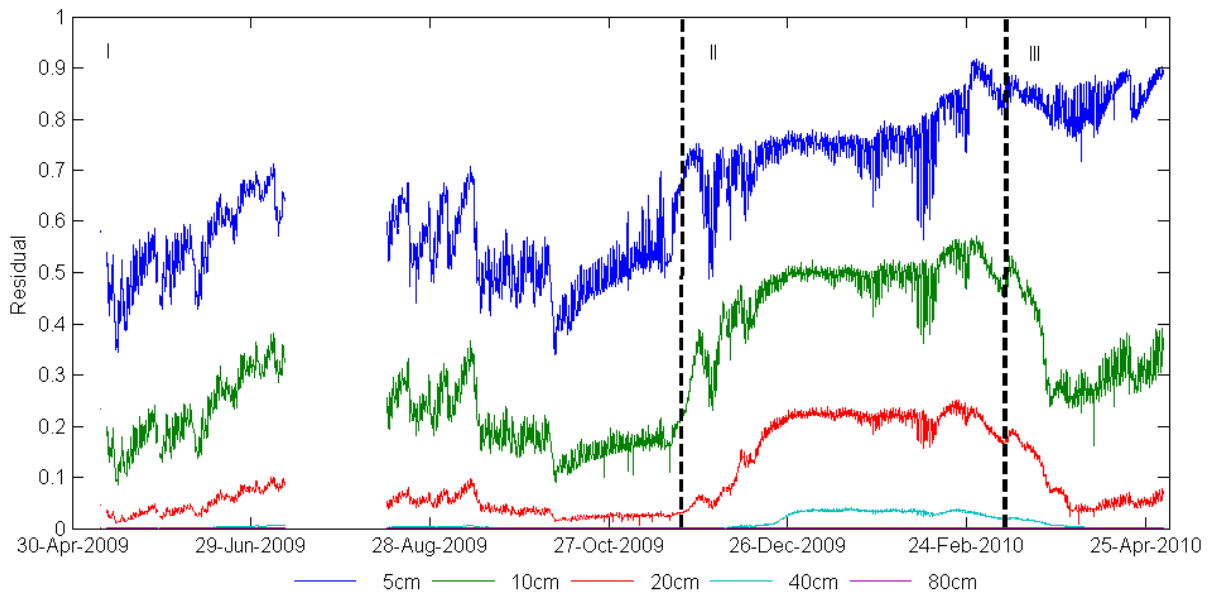


Figure C-2 The residual (see Table C-1) for each layer, with residual refers to the percentage of T_{eff} signals from deeper layers contributing to the result, as the land surface is reached.

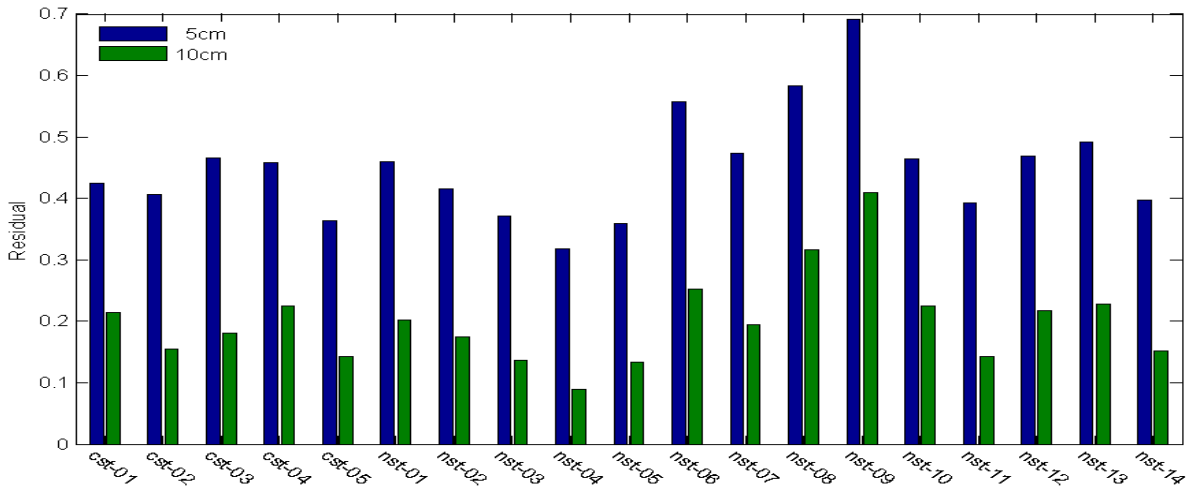


Figure C-3 The residual for each site for the first two layers as in Figure C-2.

It can be inferred that, in order to estimate T_{eff} as accurately as possible, the physical mounting depth should be designed to minimize the residual as much as possible. To provide a proof of concept calculation, the same mounting depth was used throughout the Maqu Network, with $\Delta x_1 = 5 \text{ cm}$ for the first and $\Delta x_2 = 10 \text{ cm}$ for the second layer. For each site, the residual of weights for the second layer ($\prod_{j=1}^1 e^{-B_j}$, the middle layer as in Table C-1) is shown in blue bars, while green bars represent the third layer ($\prod_{j=1}^2 e^{-B_j}$, the deepest layer as in Table C-1, Figure C-3). The smaller residual signal in Figure C-3 indicates the smaller error of each site in estimating T_{eff} . Figure C-3 shows that the NST-04 site is relatively reliable, with an error in estimating T_{eff} of less than 10%. This means that, based on the 5 cm and 10 cm installation configuration, the NST-04 site can be used to calculate T_{eff} representatively, especially when compared to other sites in the Maqu Network (Figure C-3).

Table C-2 Weight Functions for each station based on the Lv scheme

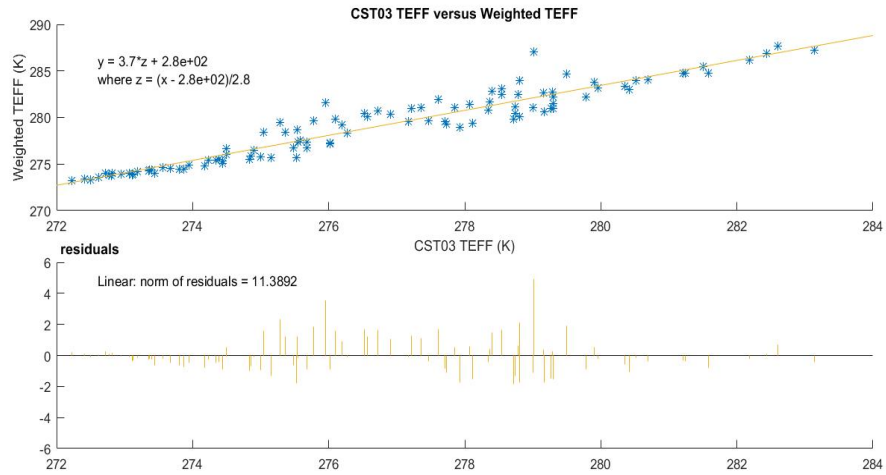
Station Name	Station Normalized Residual Signal	Weights
CST03	0.773499	0.14742
CST05	0.867363	0.168308
NST01	0.722788	0.165309
NST03	0.883096	0.137755
NST06	0.600393	0.114428
NST07	0.741575	0.141335
NST08	0.441673	0.084178
NST09	0.216526	0.041267
Sum	5.246913	1

Appendix D: ECMWF-ECOCLIMAP Vegetation classification as adopted in CMEM

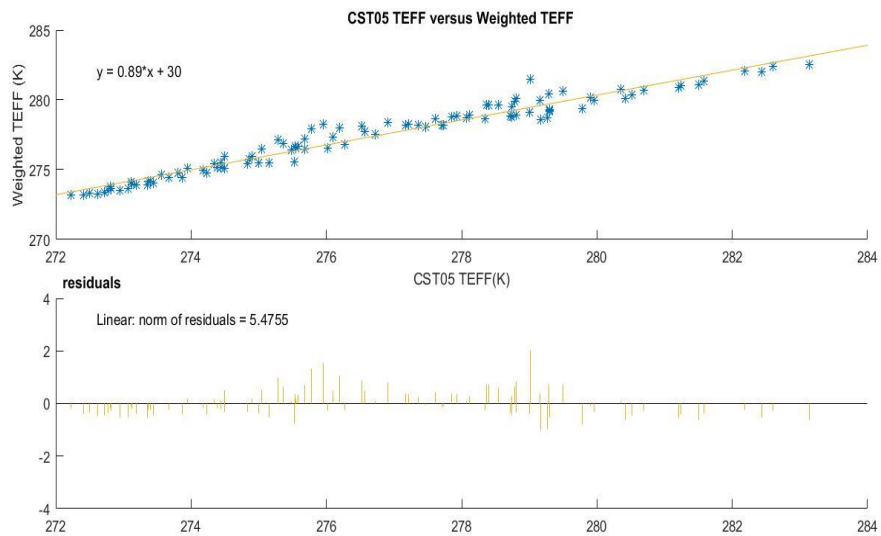
Table 10: Vegetation classification for ECMWF-Ecoclimap

No vegetation		0
High vegetation	Deciduous forests	1
	Coniferous forests	2
	Rain forests	3
Low vegetation	C3 grasslands	4
	C4 grasslands	5
	C3 crops	6
	C4 crops	7

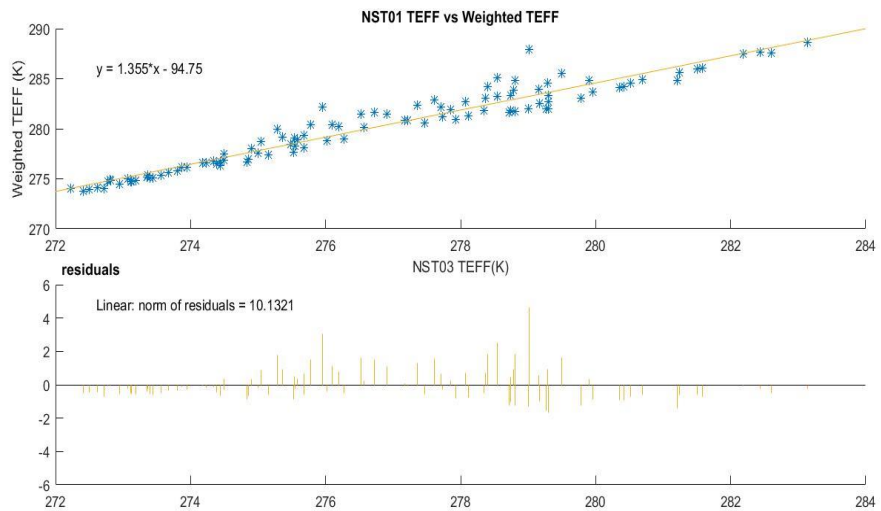
Appendix E: Residual error between individual stations TEFF and Weighted TEFF



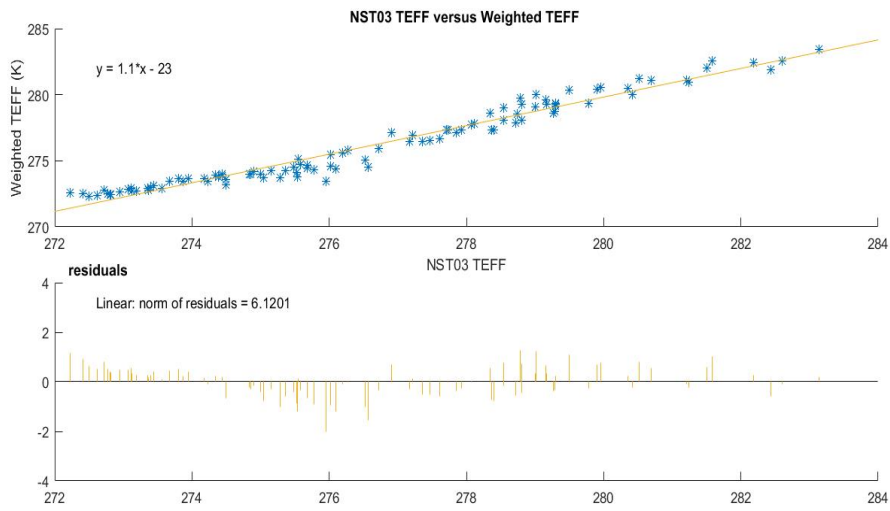
1.



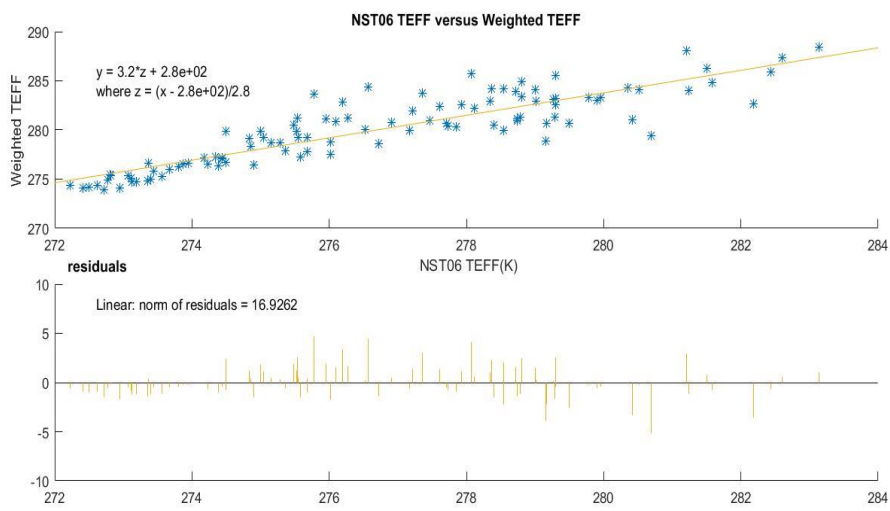
2.



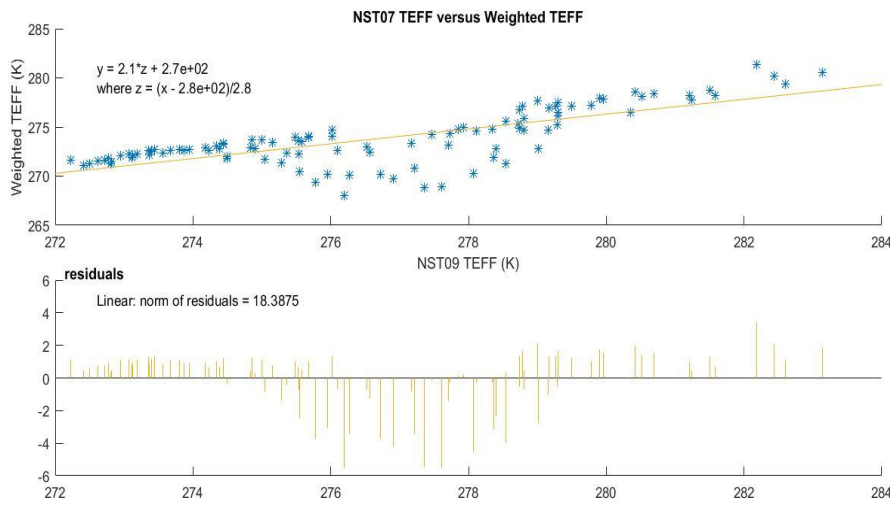
3.



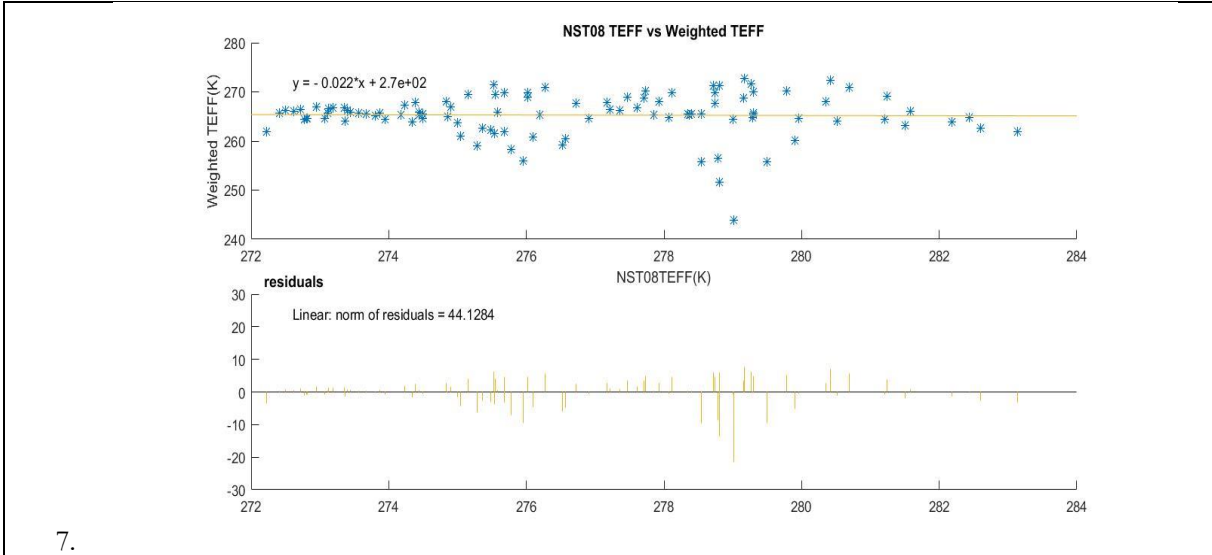
4.



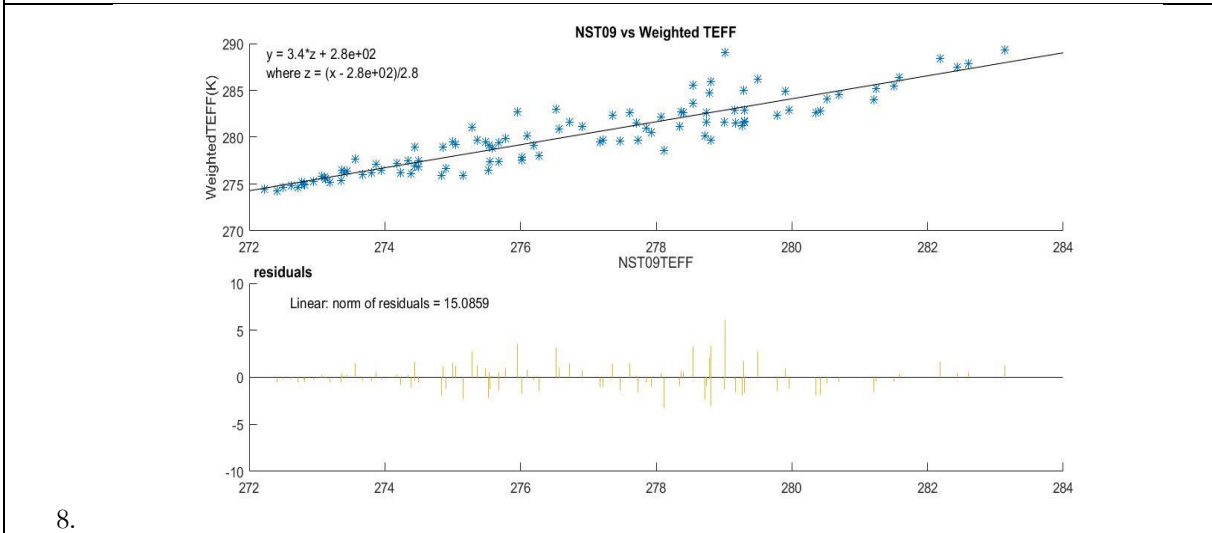
5.



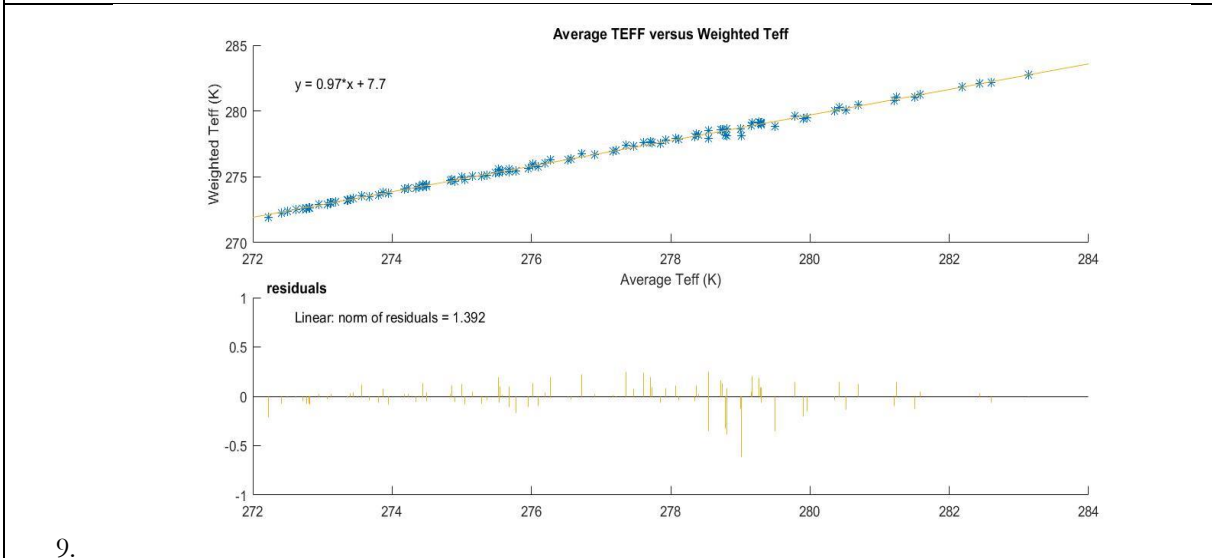
6.



7.



8.



9.

Figure 22: Norm of residuals for individual stations

Appendix F: Scatter plots for matchup between SMAP TB (H and V) and weighted model outputs

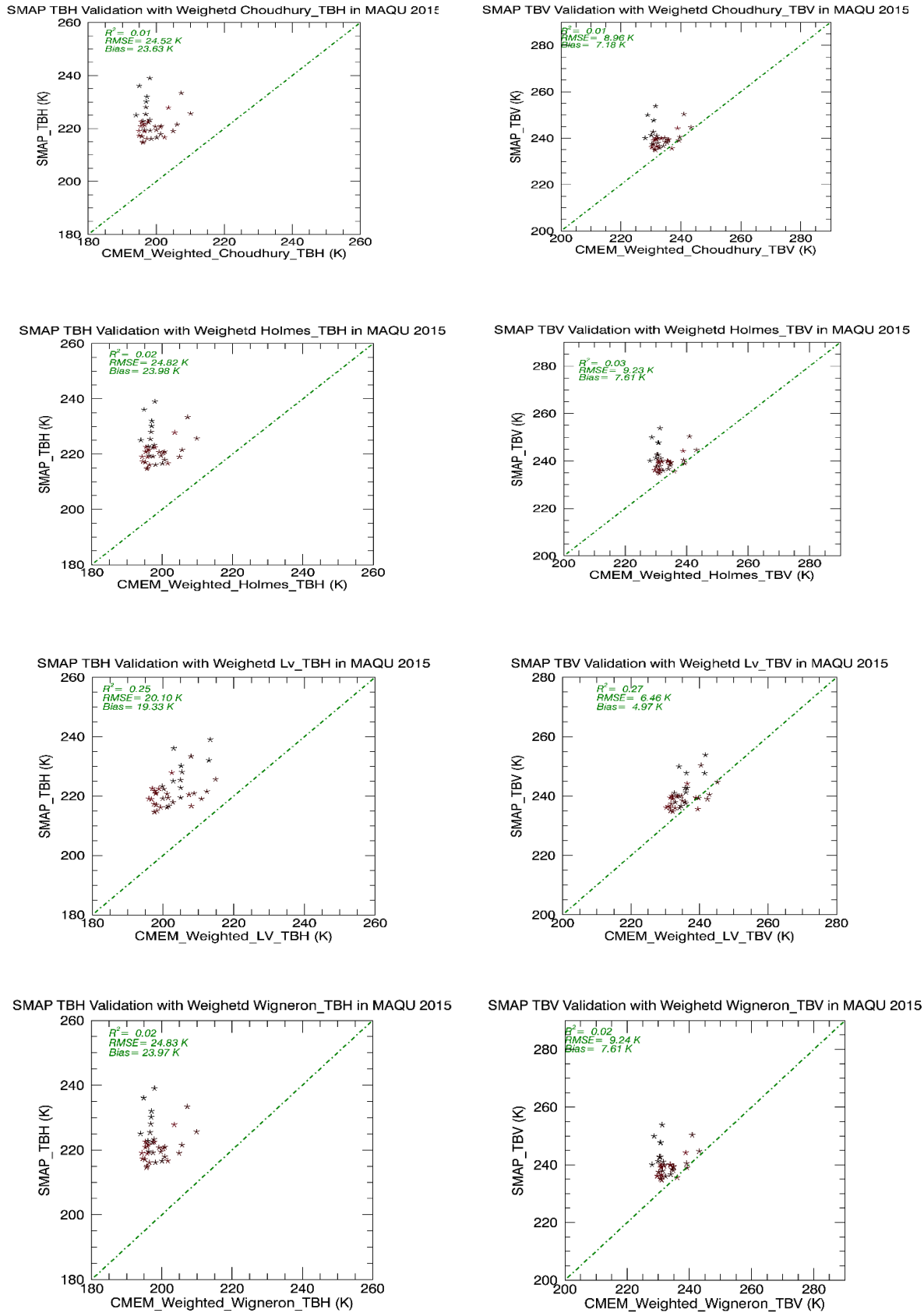


Figure 23: Scatter plots of SMAP TB against Weighted TEFF

Appendix G: Scatter plots for matchup between SMAP TB (H and V) and a model outputs

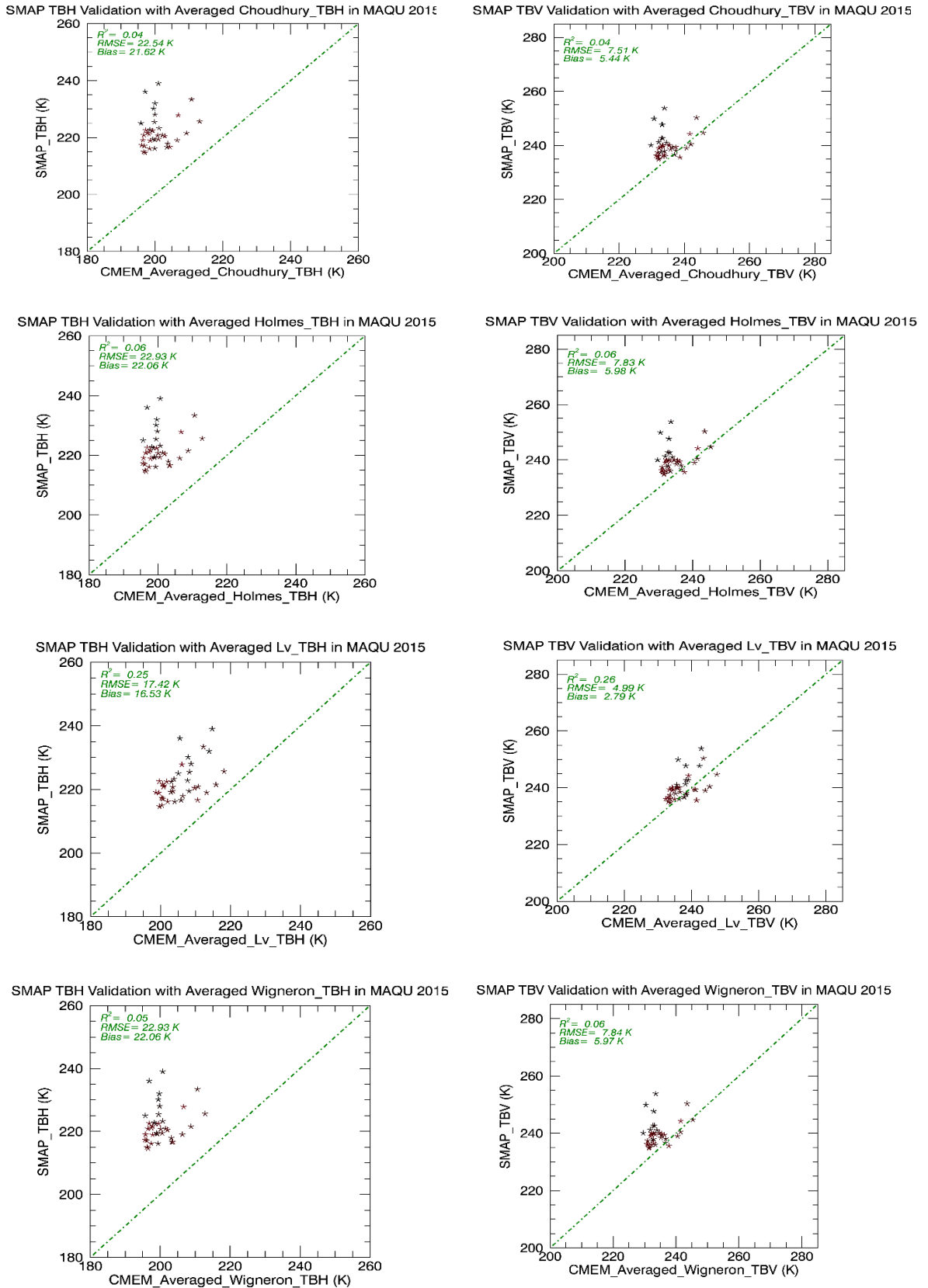


Figure 24: Scatter plots of SMAP Tb versus Simple Average TEFF